The compositional engineering of organicinorganic hybrid perovskites for highperformance perovskite solar cells

Wenzhan Xu, Xiang Yao, Haodong Wu, Tao Zhu & Xiong Gong

Emergent Materials

ISSN 2522-5731 Volume 3 Number 6

emergent mater. (2020) 3:727-750 DOI 10.1007/s42247-020-00128-8



Your article is protected by copyright and all rights are held exclusively by Qatar **University and Springer Nature Switzerland** AG. This e-offprint is for personal use only and shall not be self-archived in electronic repositories. If you wish to self-archive your article, please use the accepted manuscript version for posting on your own website. You may further deposit the accepted manuscript version in any repository, provided it is only made publicly available 12 months after official publication or later and provided acknowledgement is given to the original source of publication and a link is inserted to the published article on Springer's website. The link must be accompanied by the following text: "The final publication is available at link.springer.com".



Author's personal copy

Emergent Materials (2020) 3:727–750 https://doi.org/10.1007/s42247-020-00128-8

REVIEW



The compositional engineering of organic-inorganic hybrid perovskites for high-performance perovskite solar cells

Wenzhan Xu¹ · Xiang Yao² · Haodong Wu¹ · Tao Zhu¹ · Xiong Gong¹

Received: 5 September 2020 / Accepted: 23 September 2020 / Published online: 2 November 2020 © Qatar University and Springer Nature Switzerland AG 2020

Abstract

In the last decade, organic–inorganic perovskite materials have drawn great attentions in both academic and industrial sectors because of their remarkable optoelectronic and photovoltaic properties. Various perovskite materials have been investigated for high-performance perovskite solar cells. In this short review, we aim to illustrate optimized photovoltaic properties of perovskite materials through compositional engineering of organic–inorganic hybrid perovskite materials. We firstly elaborate the progresses of compositional engineering for each of three components in AMX₃ perovskite materials, and then highlight the optoelectronic and photovoltaic properties of the resultant perovskite materials. It was found that the compositional engineering of organic–inorganic hybrid perovskite solar cells. Lastly, the outlook and prospects of compositional engineering of organic–inorganic hybrid perovskite materials are briefly discussed.

1 Introduction

Organic–inorganic hybrid perovskites with a chemical formula of AMX₃, where A is CH₃NH₃¹⁺ (MA¹⁺), or NH₂CH=NH₂¹⁺ (FA¹⁺), or Cs⁺, M is Pb²⁺ or Sn²⁺, and X is C Γ , or Br Γ , or Γ or their combination, have been rapidly developed for approaching efficient perovskite solar cells (PSCs) due to their distinctively optoelectronic properties, such as narrow band gaps, high absorption coefficient, long charge carrier diffusion length, and low exciton binding energy [1–4]. In 2009, Miyasaka and co-workers firstly reported MAPbX₃ (where X is Γ or Br Γ) perovskites as the sensitizers in the dye-sensitized solar cells, which paved a way for using organic–inorganic hybrid perovskites as the light harvesters in photovoltaics [5]. After that, great efforts have

Wenzhan Xu, Xiang Yao and Haodong Wu contributed equally to this work.

- School of Polymer Science and Polymer Engineering, College of Engineering and Polymer Science, The University of Akron, Akron, OH 44325, USA
- Tianjin Key Laboratory of Molecular Optoelectronic Sciences, School of Science, Tianjin University & Collaborative Innovation Centre of Chemical Science and Engineering, Tianjin 300072, People's Republic of China

been dedicated in development of efficient PSCs, and power conversion efficiencies (PCEs) have been rapidly boosted from initial 3.8 to 25.2% [6–8]. Nowadays, studies demonstrated that PSCs possess greatest potentials to compete with some established solar cell technologies, such as silicon, copper indium gallium selenide (GIGS), cadmium telluride (CdTe), and gallium arsenide (GaAs) [9].

Optimization of device architectures including mesoscopic device structure [10, 11], planar heterojunction [12–14], and bulk heterojunction device structures [15–17], interface engineering (surface passivation) [18], and processing engineering (hot casting, additive doping, thermal annealing) [17, 18] have been attempted to boost PCEs of PSCs. On the other hand, many approaches have been focused on the development of novel hybrid perovskite materials and charge transport materials [19–22].

Based on the crystal structures, hybrid perovskite materials are cataloged as three-dimensional (3D) and two-dimensional (2D) perovskite materials. 3D perovskite materials are with calcium titanium oxide (CaTiO₃) structure [23]. Unlike 3D perovskites AMX₃, 2D perovskite materials, including pure-2D and quasi-2D structures, have a general formal of (RH₃)₂A_{n-1}M_nX_{3n+1} (n=1, pure-2D; n=1 is definite integer, quasi-2D), which was ascribed to the tolerance factor of perovskites beyond the ideal range as introduction of large ionic radius organic cations to break the symmetry of structures [24, 25]. Then, 2D perovskites have various orientations, such as the <100>-oriented 2D, which can be further categorized into









the Ruddlesden–Popper (RP), the Dion–Jacobson (DJ), and mixed RP:DJ layered structures. 3D perovskite materials were widely used in development of efficient PSCs due to its superior optoelectronic properties and 2D perovskite materials were applied for fabrication of stable PSCs since their good stabilities in the ambient atmosphere and structural tunability.

The crystallographic stability of 3D perovskite materials with a CaTiO₃ crystal structure [26, 27] is determined by the Goldschmidt tolerance factor (t), which is described as $t = (R_A)$ $+R_X$)/ $[\sqrt{2(R_M+R_X)}]$, where R_A , R_M , and R_X are the ionic radii of the respective ions [28–30]. An ideal cubic crystal structure could be formed as t = 1, while the ideal cubic system will transfer to a distorted structure as 0.8 < t < 1. A smaller t value indicates that the symmetry of crystal structures is reduced, resulting in the formation of less symmetric tetragonal or orthorhombic structures. Moreover, the different A cations with various ionic sizes could give rise to the phase transition in 3D perovskite structure. The phase transformation is mainly reflected in the changed M-X-M angle of the corner-sharing [MX₆]⁴⁻ octahedral and the angle will change from an ideal angle of 180° to 150° [31]. But the distortion of octahedra could not change 3D frameworks architecture [32]. According to the nomenclature [33], the undistorted perovskite structure is named α -phase. After the first and second phase transitions, the distorted perovskite structure is termed as β -phase and γ -phase, respectively. These α -, β -, and γ phases are collectively termed as the black phase. But, as the A cation is too small or too large, the preferred structures will be chain-like NH₄CdCl₃-type and CsNiBr₃-type structures with lower dimensionality, instead of a normal 3D perovskite structure. These chain-like structures are named as δ -phase or yellow phase [34].

Studies demonstrated that the substitution of either A-site, or M-site, or X-site by suitable ions in AMX₃ with suitable ions was a facial way to tune physical properties of the resultant perovskite materials, thus to boost device performance of PSCs [35, 36]. Such substitution could tune the formation of the black phase, and the band gaps, charge transport properties, and film morphologies of the resultant perovskite materials [37, 38]. In this short review, we will highlight the compositional engineering of tuning band gaps, optoelectronic properties, and photovoltaic properties of perovskite materials. The compositional engineering on 2D perovskite materials were overviewed in our recently publication [39] and others [40, 41].

2 Organic or inorganic A-site cations

Either organic or inorganic A-site cations are indispensable elements in the formation of 3D frameworks of hybrid perovskite materials. A-site cation determines the perovskite phase structure, the perovskite phase stability, and the optoelectronic







properties of 3D perovskite materials [42, 43]. Moreover, the A-site cation plays a major role in achieving desirable lattice; otherwise, the unmatched A-site cation will distort the whole lattice. The long-chain organo-ammonium ligands are introduced into the structure to form 2D perovskites. Thus, the optical and electrical properties of the resultant perovskites were dramatically changed [44]. So far, most of efficient PSCs were reported from mixed monovalent cations (MA/FA/Cs) 3D perovskite materials, but MA-based perovskite materials exhibited poor stability due to poor moisture stability of the MA cation and the reversible phase transition between the tetragonal and cubic structure at 57 °C. Thus, partial substitution of the MA cation by FA, Cs, Rb, or mixed cations would be a facile way to address stability issues [45].

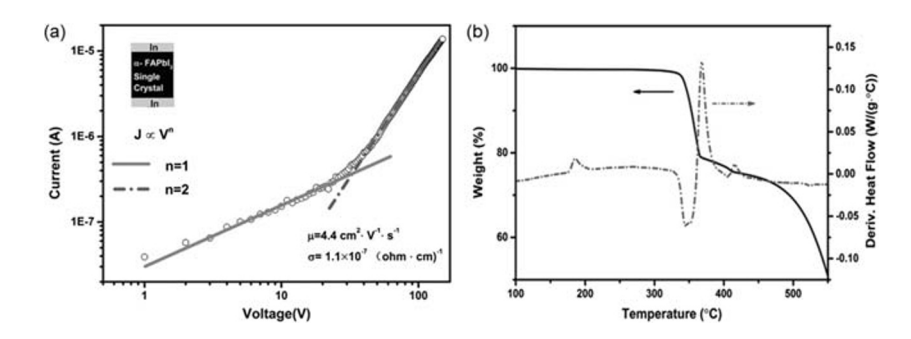
2.1 FAMX₃-type perovskites

FA cation has a slightly larger ionic radius than that of the MA cation, which could lead to the increase in the tolerance factor t of FA-based perovskites. The substitution of the A-site cation could induce the modification of the M-X bond angle and the bond length, which would alter the band gaps and crystal structures of 3D perovskite materials. FAPbI₃ has been widely applied in PSCs due to its distinguished advantages, such as larger FA cation could form more symmetric crystal structure. In addition, FA-based perovskites have smaller band gaps and possess superior thermal stability [46, 47].

As indicated in Fig. 1a, Yang et al. reported FAPbI₃ single crystal exhibiting the electrical conductivity of $1.1 \times 10^{-7} \Omega$ cm $^{-1}$, which was one order of magnitude higher than that (1 × $10^{-8} \,\Omega \,\mathrm{cm}^{-1}$) observed from MAPbI₃ single crystal [48]. They further reported the phase transition temperature of FAPbI₃ single crystal from δ -phase to α -phase was at 185 °C, with a color change from yellow to black, as shown in Fig. 1b. It was also reported that the phase transition temperature of FAPbI₃ single crystal was at 150 °C [49]. Such temperature difference for the phase transition temperature within FAPbI₃ single crystal was probably originated from the quality of single crystal prepared by different fabrication methods [48, 49]. Moreover, FAPbI₃ single crystal exhibited a high charge carrier mobility of 4.4 cm² V⁻¹ s⁻¹ and a long charge carrier lifetime of 484 nanosecond (ns). The studies further demonstrated that FAPbI₃ single crystal has good optical and electrical properties, which are suitable for approaching efficient PSCs.

Baikie and co-workers firstly reported PSCs by FAPbI₃ [50]. As indicated in Fig. 2a, PSCs by FAPbI₃ exhibited a short-circuit photocurrent ($J_{\rm SC}$) of 6.45 mA/cm², an open-circuit voltage ($V_{\rm OC}$) of 0.97 V, a fill factor (FF) of 68.7%, and with a corresponding PCE of 4.30%. It was found that the black phase coexisting with the yellow phase was easily formed as precursor solution was thermally annealing at 60 °C. Such mixed phases hindered the electron transport within

Fig. 1 a Dark current–voltage curve of α -phase single crystal FAPbI $_3$ for space charge-limited current analysis. b TGA-DSC curves of single crystal FAPbI $_3$. Reprinted with permission from ref. [48] Copyright 2016 WILY-VCH



FAPbI₃. Thus, PSCs by FAPbI₃ exhibited a poor PCE. As indicated in Fig. 2b, based on the optical absorption measurements, a band gap of FAPbI₃ was estimated to be ~ 1.47 eV.

Further studies indicated that FAPbI₃ displayed black phase with the trigonal symmetry and the yellow non-perovskite phase with the hexagonal symmetry.

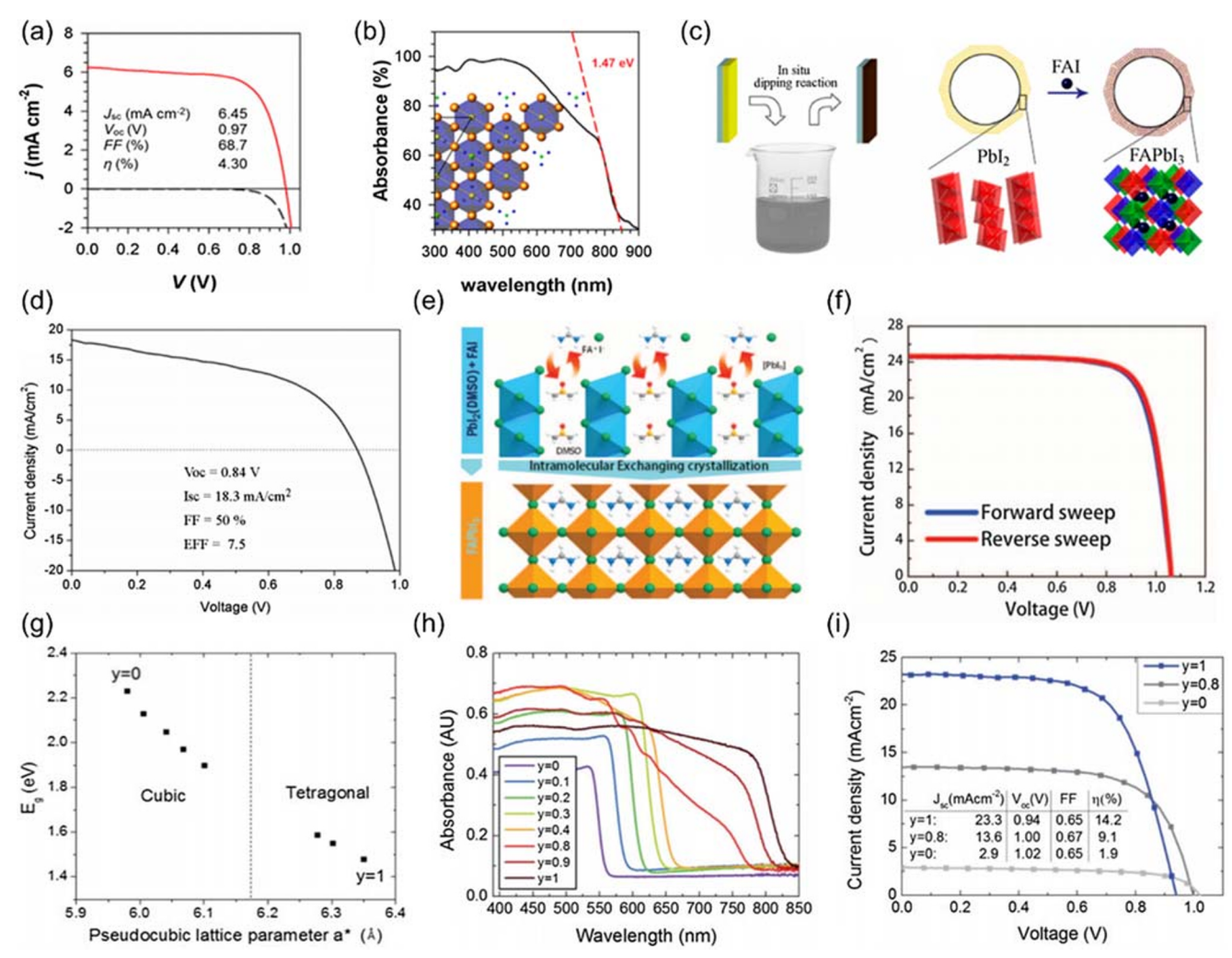


Fig. 2 a The J–V curve for the FAPbI₃ device under AM1.5G illumination and dark conditions. **b** The absorption spectrum of FAPbI₃ perovskite deposited on quartz substrate. Reprinted with permission from ref. [50] Copyright 2013 American Chemical Society. **c** Schematic illustration of in situ formation of FAPbI₃ by in situ dipping reaction of PbI₂ and FAI on the TiO₂ surface. **d** The J–V curve of the as-fabricated FAPbI₃ solar cells. Reprinted with permission from ref. [51] Copyright 2014 American Chemical Society. **e** Schematics of FAPbI₃ perovskite crystalization involving the direct intramolecular exchange of DMSO. **f** The J–

V curves of best device measured with a 40-ms scanning delay in reverse and forward modes. Reprinted with permission from ref. [52] Copyright 2015 Science (AAAS). **g** The variation of band gap with pseudo-cubic lattice parameter as determined from XRD spectra. **h** UV–Vis absorption spectrum of the FAPbI_yBr_{3-y} perovskites with varying *y*. **i** The J–V characteristics of FAPbI_yBr_{3-y} perovskite solar cells. Reprinted with permission from ref. [53] Copyright 2015 the Royal Society of Chemistry





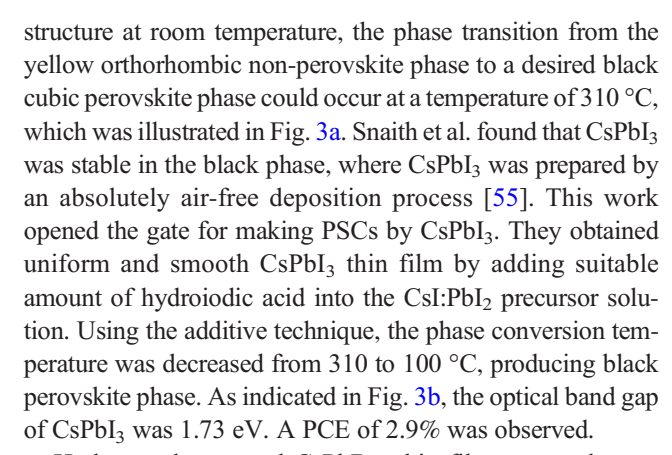


It was also found that the formation of the FAPbI₃ perovskite thin film dependent on the substrates and synthetic methods [51, 52, 54]. Cui et al. reported a facile way to deposit FAPbI₃ thin films onto the mesoporous TiO₂ (mp-TiO₂) layer via a two-step method [51]. Pure-phase FAPbI₃ perovskite thin film can be obtained as it was deposited at a temperature of 100 °C, as shown in Fig. 2c. Moreover, a PCE of 7.5% was observed from PSCs by FAPbI₃ perovskite thin film incorporated with poly(3-hexylthiophene-2,5-diyl) as the hole transport layer (HTL) in Fig. 2d. The mp-TiO₂ layer was also important for improving the charge carrier collection efficiency, which could result in enlarged FF and $V_{\rm OC}$. Seok et al. reported a method for deposition of dense and uniform FAPbI₃ thin film, which was involved an intramolecular exchange process, converting both PbI₂ and FAI into FAPbI₃ thin film, as illustrated in Fig. 2e [52]. This process contributed to high-quality FAPbI3 thin film with oriented perovskite crystals, uniform and dense microstructures, and without residual PbI₂. PSCs by FAPbI₃ thin film prepared by above method exhibited a PCE of 19%, with excellent reproducibility, as shown in Fig. 2f.

Studies demonstrated that the band gaps of perovskite materials can be tuned by adjusting the size of A-site cations [53]. For example, as the ionic radius of A-site cation is gradually increased, the band gaps of perovskites are gradually decreased from 1.73 eV (CsPbI₃) to 1.57 eV (MAPbI₃), and then further to 1.48 eV (FAPbI₃). Snaith et al. reported FAPbI_xBr₃. with tunable band gaps from 1.48 to 2.23 eV through tuning the iodide fraction in FAPbI_xBr_{3-x} [53]. The phases of $FAPbI_xBr_{3-x}$ were transferred from the cubic (as x < 0.5) to the tetragonal (x > 0.7) crystal structures in Fig. 2g, h. They further reported a PCE of 14.2%, with a J_{SC} of 23 mA cm⁻² from planar heterojunction PSCs, as shown in Fig. 2i. Such enhanced PCEs was attributed to a small amount of hydroiodic acid mixed with FAI:PbI₂ precursor solution, which could assist FAPbI_xBr_{3-x} to form pure phase, continuous, and uniform thin films.

2.2 CsMX₃-type perovskites

The organic components (MA or FA cations) in perovskite materials are highly hygroscopic, volatile, and can thermally decompose at ~ 200 °C. Moreover, organic–inorganic hybrid perovskites are susceptible to moisture, light, and oxygen. All these issues restricted further development of efficient and stable PSCs. To address these problems, all-inorganic perovskites were developed through substitution of organic components by cesium (Cs) [58]. For instance, CsPbBr₃ single crystal has been reported with high electron mobility (~ 1000 cm² V⁻¹ s⁻¹) and long electron lifetime (2.5 μ s) [59]. CsSnI₃ with high electron mobility (up to ~ 2300 cm² V⁻¹ s⁻¹) and hole mobility (~ 320 cm² V⁻¹ s⁻¹) was reported [56]. Although CsPbI₃ typically displayed the yellow non-perovskite



Hodes et al. reported CsPbBr₃ thin film prepared at an annealing temperature of 250 °C via two-step deposition method in an ambient atmosphere [56]. Photovoltaic performance of PSCs by CsPbBr3 thin film was comparable to that by MAPbBr₃ thin film [60, 61]. CsPbBr₃ exhibited a band gap of 2.36 eV, which was close to that (2.32 eV) for MAPbBr₃. The maximum $V_{\rm OC}$ of 1.28 eV and the maximum PCE of 5.95% were observed from PSCs with a device architecture of FTO/compact TiO₂ (c-TiO₂)/mp-TiO₂/CsPbBr₃/PTAA/ Au, as shown in Fig. 3c, d. Liang et al. reported PSCs by CsPbBr₃ with a device structure of FTO/c-TiO₂/mp-TiO₂/ CsPbBr₃/Carbon, where CsPbBr₃ thin film was prepared in air, which exhibited PCEs in the relative humidity ranged from 90 to 95% after 2500 h operation. Ma et al. fabricated PSCs by CsPbIBr₂ thin film through dual source thermal evaporation process [57]. CsPbIBr₂ thin film possessed a band gap of 2.05 eV. As showed in Fig. 3e, f, PSCs without HTL but with post-annealing treatment exhibited a maximum PCE of 4.7%. Yip et al reported efficient and relative stable PSCs by CsPbI_{2.5}Br_{0.5} as the photoactive layer [62].

2.3 (MA)_x(FA)_{1-x}MX₃-type perovskites

As mentioned above, larger FA cation provides a possibility to decrease the band gap of perovskites toward the optimal value of 1.4 eV. The black α-phase FAPbI₃ with suitable narrow band gap of ~ 1.48 eV was unstable in ambient condition and FAPbI₃ is favorable for forming the yellow δ-phase with a wide band gap in ambient condition. The instability of the black α-phase FAPbI₃ in the ambient condition restricted its photovoltaic applications. Gratzel et al. firstly reported (MA)_x(FA)_{1-x}PbI₃ as the light harvesting layer for PSCs [63]. The mixed-organic-cation perovskites were fabricated by a two-step deposition method. The band gap of (MA)_x(FA)_{1-x}PbI₃ could be tuned by gradually substituting MA cation with FA cation. PSCs by (MA)_{0.6}(FA)_{0.4}PbI₃ thin film yielded a PCE of 14.9%.

Han et al. reported a novel strategy to prepare $(MA)_x(FA)_{1-x}PbI_3$ thin film without the yellow δ -phase $FAPbI_3$ through the formation of the $(FAI)_{1-x}$ -PbI₂ intermediate [64]. They found









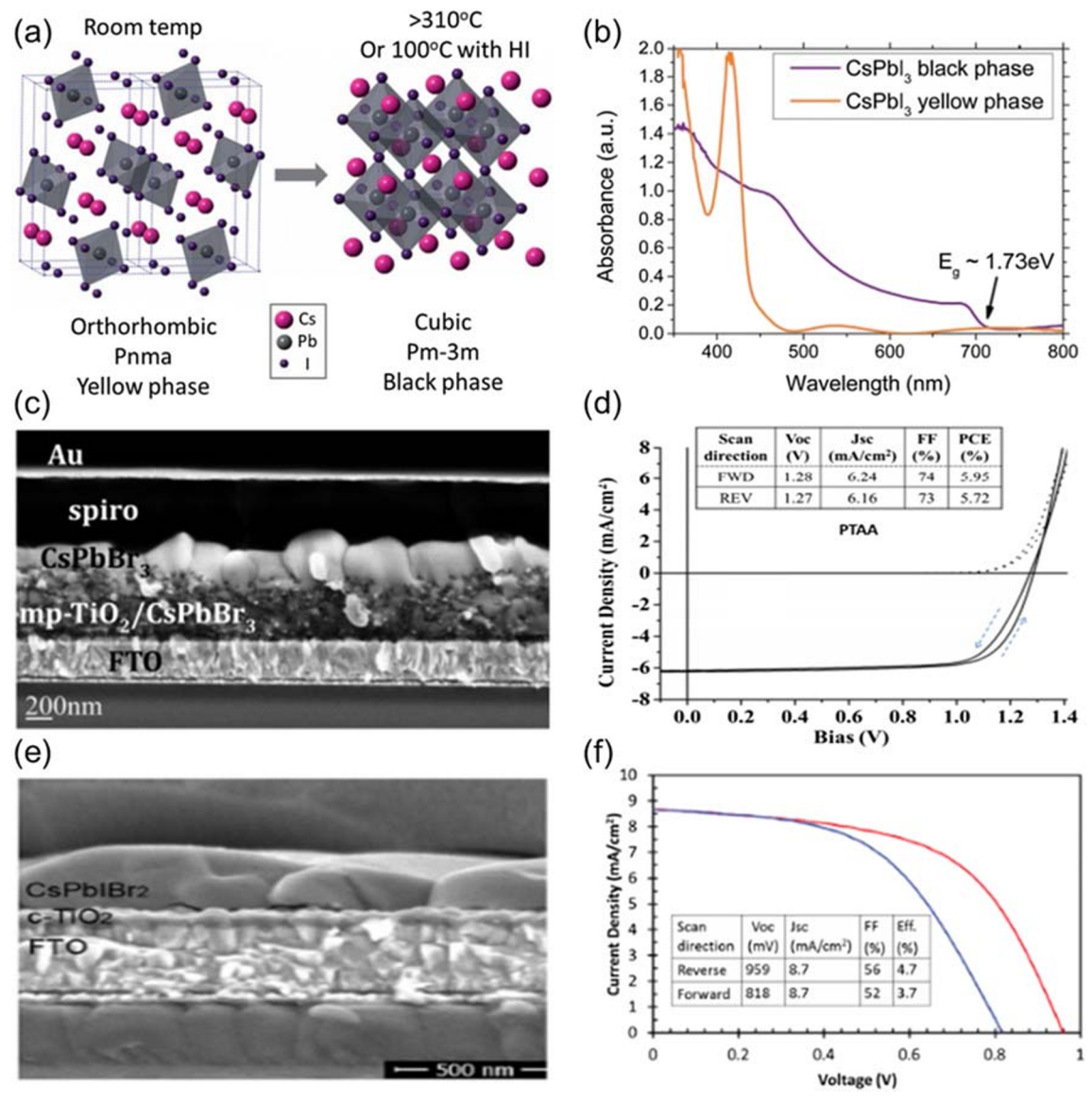


Fig. 3 a Diagrammatic structure of CsPbI₃ phases. **b** UV–Vis absorption spectrum of black and yellow phases of CsPbI₃ thin films. Reprinted with permission from ref. [55] Copyright 2015 the Royal Society of Chemistry. **c** The SEM cross-section image of the device. **d** The J–V curves and photovoltaic parameters of the as-fabricated CsPbBr₃ solar

cells. Reprinted with permission from ref. [56] Copyright 2015 American Chemical Society. **e** SEM cross-section image of the device. **f** The J–V curves of the best device in reverse and forward modes. Reprinted with permission from ref. [57] Copyright 2016 WILY-VCH

that the formation of the pure-phase $(MA)_x(FA)_{1-x}PbI_3$ through an intermediate state with a non-stoichiometric complex $((FAI)_{1-x}-PbI_2)$ as the $(MA)_x(FA)_{1-x}PbI_3$ thin film thermally annealed from 145 to 175 °C, as shown in Fig. 4a. Seok et al. reported a strategy that introducing second halide Brinto $(MA)_x(FA)_{1-x}PbI_3$ to form $(FAPbI_3)_{1-x}(MAPbBr_3)_x$ and further found that PSCs by $(FAPbI_3)_{1-x}(MAPbBr_3)_x$ exhibited over 18% PCEs, as shown in Fig. 4b, c [65]. Bi et al. also reported the development of $(FAPbI_3)_{1-x}(MAPbBr_3)_x$ thin film by spin-coating a mixed solution composing of FAI, MABr, PbI₂, and PbBr₂ onto substrates and observed 20.8% PCE, as shown in Fig. 4d, e [66]. They also found that the

remained PbI_2 in $(FAPbI_3)_{1-x}(MAPbBr_3)_x$ thin film was beneficial to improve device performance through suppressing the non-radiative recombination.

2.4 Cs_xMA_{1-x}MX₃-type perovskites

Similar to the A-site partially substitution within MAPbI₃, using Cs⁺ cation to substitute MA⁺ was also used to fabricate Cs_xMA_{1-x}PbI₃ thin films. Kim et al. reported PSCs by Cs_xMA_{1-x}PbI₃ as the light-absorbing layer [67]. Cs_xMA_{1-x}PbI₃ thin film was prepared by spin-coating a precursor solution composing of MAI, CsI, and PbI₂ into the optimal









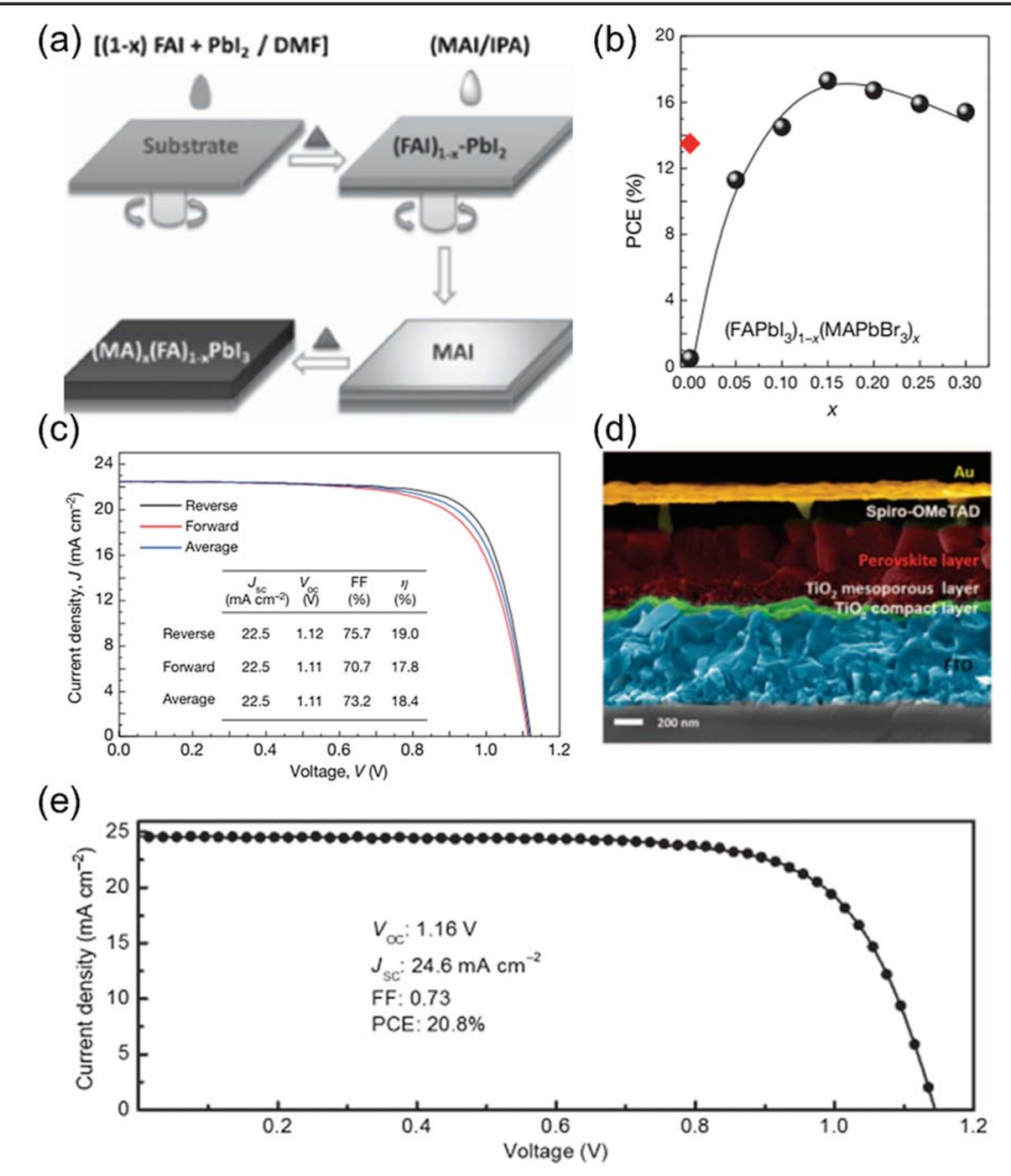


Fig. 4 a Schematic illustration of phase-pure mixed-organic-cation perovskite formation process via intermediate (FAI)_{1-x}PbI₂. Reprinted with permission from ref. [64] Copyright 2015 WILY-VCH. **b** The PCE values for solar cells fabricated with (FAPbI₃)_{1-x}(MAPbBr₃)_x. **c** The J–V curves of the device in reverse and forward modes. Reprinted with

permission from ref. [65] Copyright 2015 Nature Publishing Group. **d** The SEM cross-sectional image of the champion device. **e** The J–V curves of the best device. Reprinted with permission from ref. [66] Copyright 2016 Science (AAAS)

mixed solvent of GBL and DMF (GBL:DMF = 97:3 v/v). The optical band gap of $Cs_xMA_{1-x}PbI_3$ thin film could be easily tuned from 1.52 to 2.05 eV by controlling the ratio of the Cs cation. The band gap of $Cs_{0.1}MA_{0.9}PbI_3$ thin film was 1.52 eV and PSCs by $Cs_{0.1}MA_{0.9}PbI_3$ showed a maximum PCE of 7.68%.









2.5 Cs_xFA_{1-x}MX₃-type perovskites

To address unstable black α-phase within FAPbI₃, $MA_xFA_{1-x}PbI_3$ perovskites were developed to boost PCEs of PSCs. For example, PSCs by $(FAPbI_3)_{1-x}(MAPbBr_3)_x$ exhibited a PCE over 22% [70]. However, both FAPbI₃ and MAPbI₃ were

easily to be degraded chemically and thermally due to the hydroscopic and volatile nature of both MA⁺ and FA⁺ cations [71, 72]. But studies found out that the α-phase CsPbI₃ displayed an excellent stability at high temperature. Thus, incorporation of FAPbI₃ with CsPbI₃ was expected to have a desirable black-phase perovskite with good thermal and moisture stabilities. Park et al. reported enhanced stability of Cs_{0.1}FA_{0.9}PbI₃, which was with a band gap of 1.55 eV [68]. Cs_{0.1}FA_{0.9}PbI₃ thin film was prepared from a solution composing of CsI, FAI, and PbI₂ in DMSO. PSCs by Cs_{0.1}FA_{0.9}PbI₃ thin film exhibited a PCE of 17.1%, which was higher than that (16.3%) by FAPbI₃, as shown in Fig. 5a. It was also found that both photochemical and moisture stabilities of Cs_{0.1}FA_{0.9}PbI₃ thin film were also improved. For example, under a relative

humidity of 85%, PSCs by Cs_{0.1}FA_{0.9}PbI₃ thin film only showed 49.8% degradation after 7 h, whereas PSCs by FAPbI₃ thin film showed 77.8% degradation. In addition, as indicated in Fig. 5b, PSCs by Cs_{0.1}FA_{0.9}PbI₃ thin film exhibited better illumination stability.

Gratzel et al. reported Cs_{0.2}FA_{0.8}PbI_{2.84}Br_{0.16} thin film prepared by spin-coating precursor solution of CsI, FAI, FABr, and PbI₂ into a mixed solvent of DMSO and DMF [69]. The onset of absorption of Cs_{0.2}FA_{0.8}PbI_{2.84}Br_{0.16} thin film was 789 nm, which is corresponding to a band gap of 1.58 eV. PSCs by Cs_{0.2}FA_{0.8}PbI_{2.84}Br_{0.16} thin film exhibited a PCE of 18%, with no significantly reduced PCEs within 1000 h under illumination in ambient atmosphere, as indicated in Fig. 5c, d.

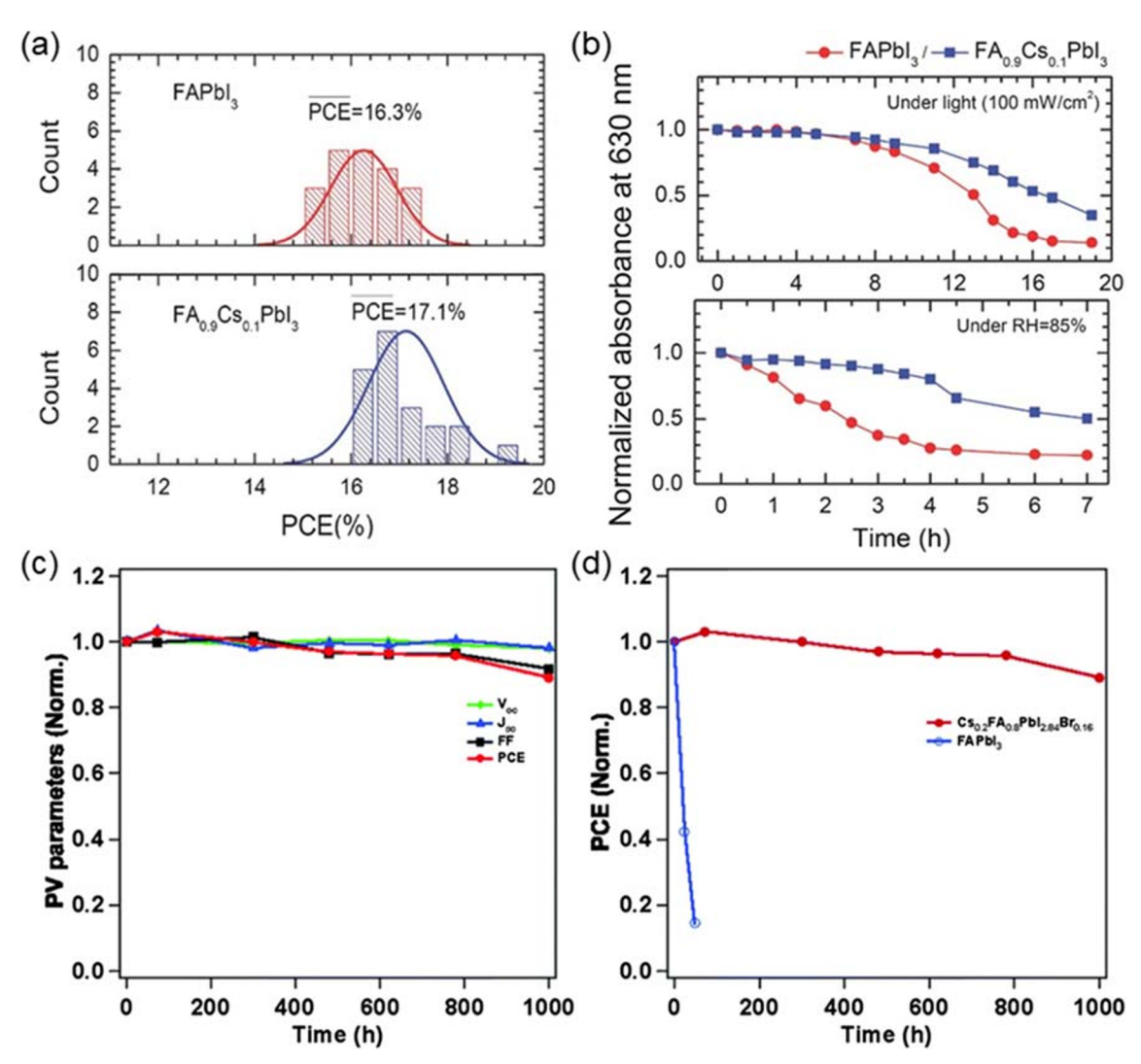


Fig. 5 a Statistical distribution of PCE of the perovskite solar cell fabricating with FAPbI₃ and FA_{0.9}Cs_{0.1}PbI₃. **b** The photostability and moisture stability test for FAPbI₃ and FA_{0.9}Cs_{0.1}PbI₃ films measured under sulfur lamp (humidity < 50%, temperature < 65%) and constant humidity of 85% in dark. Reprinted with permission from ref. [68] Copyright 2015 WILY-VCH. **c** Evolution of the photovoltaic parameters

with time for the $Cs_{0.2}FA_{0.8}PbI_{2.84}Br_{0.16}$ devices. **d** Comparison of the stability of $Cs_{0.2}FA_{0.8}PbI_{2.84}Br_{0.16}$ and $FAPbI_3$ perovskite solar cells (The unencapsulated devices were kept under ambient conditions in the dark). Reprinted with permission from ref. [69] Copyright 2016 the Royal Society of Chemistry









2.6 Cs_xMA_yFA_{1-x-y}MX₃-type perovskites

Compared with double-cation perovskites, the triple-cation (Cs/MA/FA) perovskites were firstly reported by Saliba and co-workers [73]. A small amount of Cs mixed with MA/FA cations could avoid the presence of the yellow δ -phase FAPbI₃, which could suppress impurity-induced charge carrier recombination, thus improve charge carrier transport [74]. It was found that $Cs_{0.05}(FA_{0.83}MA_{0.17})_{0.95}Pb(I_{0.83}Br_{0.17})_3$ thin film possessed excellent thermal stability. PSCs by $Cs_{0.05}(FA_{0.83}MA_{0.17})_{0.95}Pb(I_{0.83}Br_{0.17})_3$ thin film exhibited stabilized PCE of 18% under constant illumination and a maximum PCE of 21%. In addition, PSCs by $Cs_{0.05}(FA_{0.83}MA_{0.17})_{0.95}Pb(I_{0.83}Br_{0.17})_3$ thin film possessed a good reproducibility.

2.7 Cs_xRb_vMA_zFA_{1-x-v-z}MX₃-type perovskites

Saliba et al. introduced the quadruple Cs/Rb/MA/FA cations into perovskite [75]. It was found that the tolerance factor of the RbPbI₃ was at 0.78, which would lead to the formation of non-perovskite phase. The different A-site cation combinations, RbFA, RbCsFA, RbMAFA, and RbCsMAFA with different molar ratios were used to prepare $Rb_{0.05}(Cs_{0.05}(FA_{0.17}MA_{0.83})_{0.95})_{0.95}Pb(I_{0.83}Br_{0.17})_3$, which possess a band gap of 1.63 eV. PSCs by $Rb_{0.05}(Cs_{0.05}(FA_{0.17}MA_{0.83})_{0.95})_{0.95}Pb(I_{0.83}Br_{0.17})_3$ thin film exhibited a stabilized PCE of 21.6%. It was also found that a small amount of Rb mixed with MA/FA cations could avoid the presence of the PbI₂ and generate yellow δ-phase impurities in the resultant perovskites. It was also found that a small amount of Rb mixed with MA/FA cations could avoid the presence of the PbI₂ and impede the emergence of yellow δ phase impurities in the resultant perovskites [76]. As a result, PSCs by Rb/Cs/MA/FA cation-based perovskite kept 95% of its initial PCE after 500 h operational at 85 °C and under illumination.

3 The metal cation M²⁺

Lead cation (Pb^{2+}) was most widely used cation in perovskites for approaching efficient PSCs [77, 78]. However, lead is a toxic element. Thus, to seek less toxic or no-toxic alternatives to substitute Pb^{2+} cation was one of ongoing directions. N u m b e r o f h y b r i d h a l i d e p e r o v s k i t e s , $(C_4H_9NH_3)_2(CH_3NH_3)_{n-1}MI_4$, where M = Ge, Sn, Pb, have been investigated [79, 80]. Among them, many studies have been focused on the substitution of toxic Pb^{2+} with non-toxic Sn^{2+} since the ionic radius of Sn^{2+} is close to that of Pb^{2+} .









3.1 ASnX₃-type perovskites

Lead-free perovskites, such as MASnI₃, FASnI₃, and CsSnI₃, have been gradually drawn attentions in the past years [84–86]. It was found that MASnI₃ thin film was with a pseudo cubic space group P4mm at ambient conditions [87]. Whereas, the space groups of FASnI₃ were corresponding to Amm2 and Imm2 at 340K and 180K, respectively [88]. As indicated in Fig. 6a, Tao et al. found that single crystal of MASnI₃ and FASnI₃ is cubic Pm-3m space group at room temperature [81]. The band gap of MASnI₃ single crystal is approximately 1.15 eV, but the band gap of MASnI₃ polycrystalline is 1.30 eV. It was also found that FASnI₃ single crystals exhibited better stability than MASnI₃ polycrystalline in the ambient atmosphere [89].

Kanatzidis et al. firstly reported PSCs by solution-processed MASnI₃ thin film [82]. PSCs by MASnI₃ exhibited a $J_{\rm SC}$ of 16.30 mA cm⁻² and with a corresponding PCE of 5.23%, as shown in Fig. 6b. The band gap of MASnI₃ thin film is 1.30 eV, but the band gaps of MASnI_xBr_{3-x} can be tuned from 1.30 eV (MASnI₃) to 2.15 eV (MASnBr₃), as indicated in Fig. 6c. PSCs by MASnIBr₂ exhibited a $V_{\rm OC}$ of 0.88 V and a PCE of ~ 5.80%, as shown in Fig. 6d.

Snaith et al. reported PSCs by the lead-free hybrid perovskite through spin-coating of a precursor solution composing of MAI and $\rm SnI_2$ (equimolar) in DMF [90]. MASnI₃ thin film exhibited a large onset at ~ 1000 nm, which was corresponding to a band gap of 1.23 eV. PSCs by MASnI₃ thin film exhibited an approximately PCE of 6% and a $V_{\rm OC}$ of 0.88 V. Kanatzidis et al. reported a novel strategy to prepare high-quality MASnI₃ thin film from different solvents, such as DMF, DMSO, and GBL, as indicated in Fig. 6e [83]. It was found that DMSO-derived MASnI₃ thin film possessed the smallest band gap of 1.3 eV and an absorption onset at 950 nm. Thus, PSCs by DMSO derived MASnI₃ thin film exhibited a $J_{\rm SC}$ of 21.4 mA cm⁻² as shown in Fig. 6f.

Mathews et al. reported FASnI₃ thin film from FASnI₃ precursor solution mixed 20 mol% of SnF₂ for restricting the oxidation of Sn²⁺ to Sn⁴⁺ [91]. However, as indicated in Fig. 7a, a severe phase separation occurred in FASnI₃ thin film due to the addition of a high concentration of SnF₂. The FASnI₃ thin film has a 1.41 eV of band gap and PSCs by above FASnI₃ thin film exhibited a high J_{SC} of 24.45 mA cm⁻², as shown in Fig. 7b. In order to prepare dense and uniform FASnI₃ thin film, Seok et al. reported a one-step spin-coating process using a mixed solvent (DMF/DMSO [4:1 v/v]) [92]. But PSCs by FASnI₃ thin film prepared with above method only exhibited a moderate PCE of ~ 4%, as indicated in Fig. 7c, d.

CsSnI₃, CsSnBr₃, and CsSnCl₃ have been investigated due to their better stability and unique optoelectronic properties [95, 96]. Bhargava and Peedikakkandy studied the optical and structural characteristics of a variety of CsSnX₃ [93].

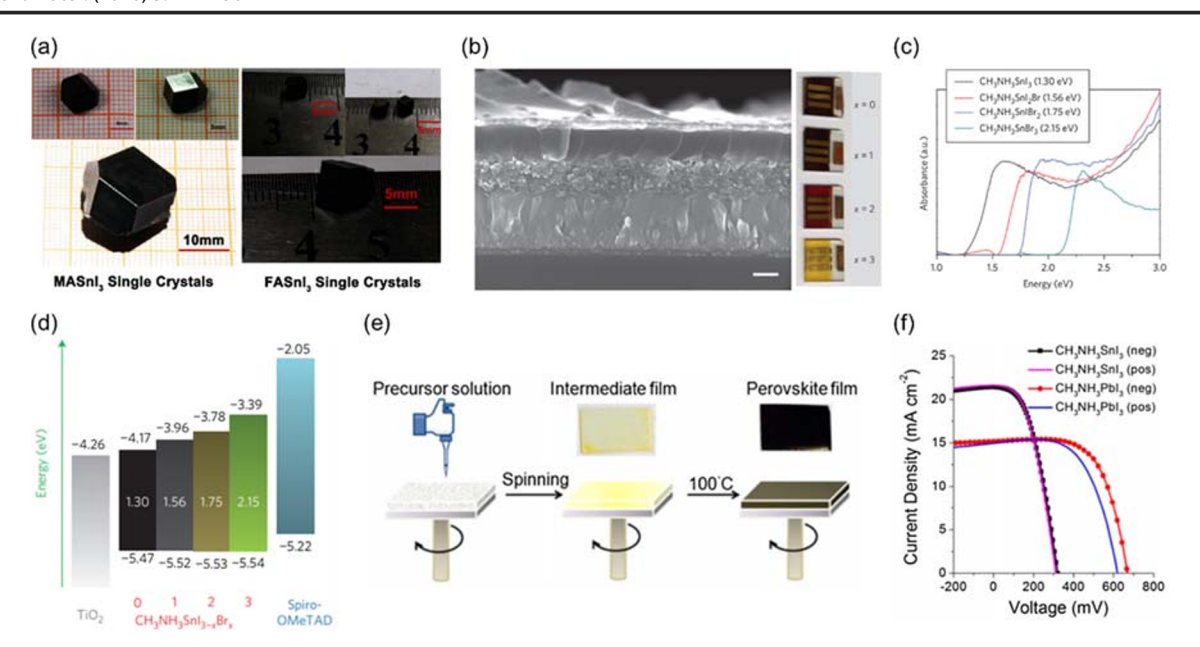


Fig. 6 a The images of single crystals for MASnI₃ and FASnI₃. Reprinted with permission from ref. [81] Copyright 2016 WILY-VCH. **b** SEM cross-sectional image of the device with MASnI₃ perovskites. **c** Absorption spectrum of the MASnI_{3-x}Br_x (x = 0, 1, 2, 3) perovskites. **d** Schematic energy-level diagram of $MASnI_{3-x}Br_x$ (x = 0, 1, 2, 3) perovskites with TiO2 and spiro-OMeTAD. Reprinted with permission from

ref. [82] Copyright 2014 Nature Publishing Group. e Schematic illustration of spin-coating process via DMSO solvate intermediate and image of as-prepared films before and after annealing process. f The J-V curves of the device employing MASnI₃ and FASnI₃ in reverse and forward modes. Reprinted with permission from ref. [83] Copyright 2015 American Chemical Society

They prepared CsSnX₃ thin film with different halide compositions, such as CsSnI₃, CsSnBr₃, CsSnCl₃, CsSnI₂Br, CsSnIBr₂, CsSnBr₂Cl, and CsSnBrCl₂ by spin-coating precursor solutions composing of mixed cesium halide and tin halide with different stoichiometric ratios in DMF. As indicated in Fig. 8a, b, the band gaps of CsSnX₃ were blue-shifted from 1.31 to 2.80 eV as halide anion was varied from I to Br and then to Cl.

Mathews et al. reported PSCs by CsSnI₃ thin film prepared at low temperature (70 °C) [94], exhibiting a J_{SC} of 22 mA cm⁻², as shown in Fig. 8c, which was dramatically lower than a theoretical value (J_{SC} of 34.3 mA cm⁻²), as shown in Fig. 8d. Such low J_{SC} was attributed to its intrinsic p-type conductivity, which could result in severe photogenerated charge carrier recombination in PSCs by CsSnI₃ [97].

3.2 AM_{1-x}Pb_xX₃-type perovskites

Ogomi et al. reported the development of MASn_xPb_{1-x}I₃ thin film by utilization of small amount of Sn²⁺ to substitute Pb²⁺ and found out that such substitution could retard the oxidation of Sn²⁺ to Sn⁴⁺ and extend absorption from 1000 to 1200 nm [98]. As indicated in Fig. 9a, the band gaps of MASn_xPb_{1-x}I₃ thin films were depended on the variation of Sn/Pb ratio. Moreover, MASn_xPb_{1-x}I₃ perovskites with high Sn ratio could increase the photoexcited charge carrier recombination [101]. PSCs by MASn_{0.5}Pb_{0.5}I₃ thin film exhibited a V_{OC} of 0.42 V, an FF of 0.50, a J_{SC} of 20.04 mA cm⁻², and with a corresponding PCE of 4.18% [98]. High $J_{\rm SC}$ was attributed to the extended absorption (1060 nm) of MASn_{0.5}Pb_{0.5}I₃ thin film.

Kanatzidis et al. also reported MASn_{1-x}Pb_xI₃ thin films prepared from a precursor solution composing of MAI, PbI₂ and SnI₂ with certain stoichiometric proportions in an aqueous solution of HI/H₃PO₂ (4:1 V/V) [99]. As indicated in Fig. 9b, c, both crystal structures and band gaps were changed with x values. PSCs by MASn_{0.5}Pb_{0.5}I₃ thin film prepared by above method showed a PCE of 7.27%.

Jen et al. reported binary metal MAPb_{1-v}Sn_vI_xCl_{3-x} perovskites [100]. MAPb_{1-v}Sn_vI_xCl_{3-x} thin films possessed uniform and dense surface coverage and high-quality crystallinity compared to pure tin-based perovskite thin films. Furthermore, the absorption edge was red-shifted from 800 nm for single leadbased perovskites to 900 nm for the binary metal perovskites, as indicated in Fig. 9d. PSCs by MAPb_{0.85}Sn_{0.15}X₃ thin film exhibited a PCE of ~ 10%. In addition, Malavasi et al. reported the synthesis and optical properties of MASn_{1-x}Pb_xBr₃ perovskites [102]. It was found that MASn_{1-x}Pb_xBr₃ thin film possessed extended NIR absorption.

PSCs by lead-based perovskites where Pb2+ was partially substituted by either Co²⁺ or Nd³⁺ were also reported [35, 36, 103]. In 2018, Gong's group reported efficient PSCs by Co²⁺ partially substituted perovskites [36]. As indicated in Fig. 10a, Pb²⁺ was indeed partially substituted by Co²⁺. Interestingly, it was found that the electrical conductivities and the Seebeck coefficients of Co²⁺ partially substituted perovskites were tuned with the Co/Pb ratio, as shown in Fig. 10b. Figure 10c presents the J-V characteristics of PSCs by either MAPb_{0.9}Co_{0.1}I₃ thin film or MAPbI₃ thin film. It was found that PSCs by MAPb_{0.9}Co_{0.1}I₃ thin film not only exhibited









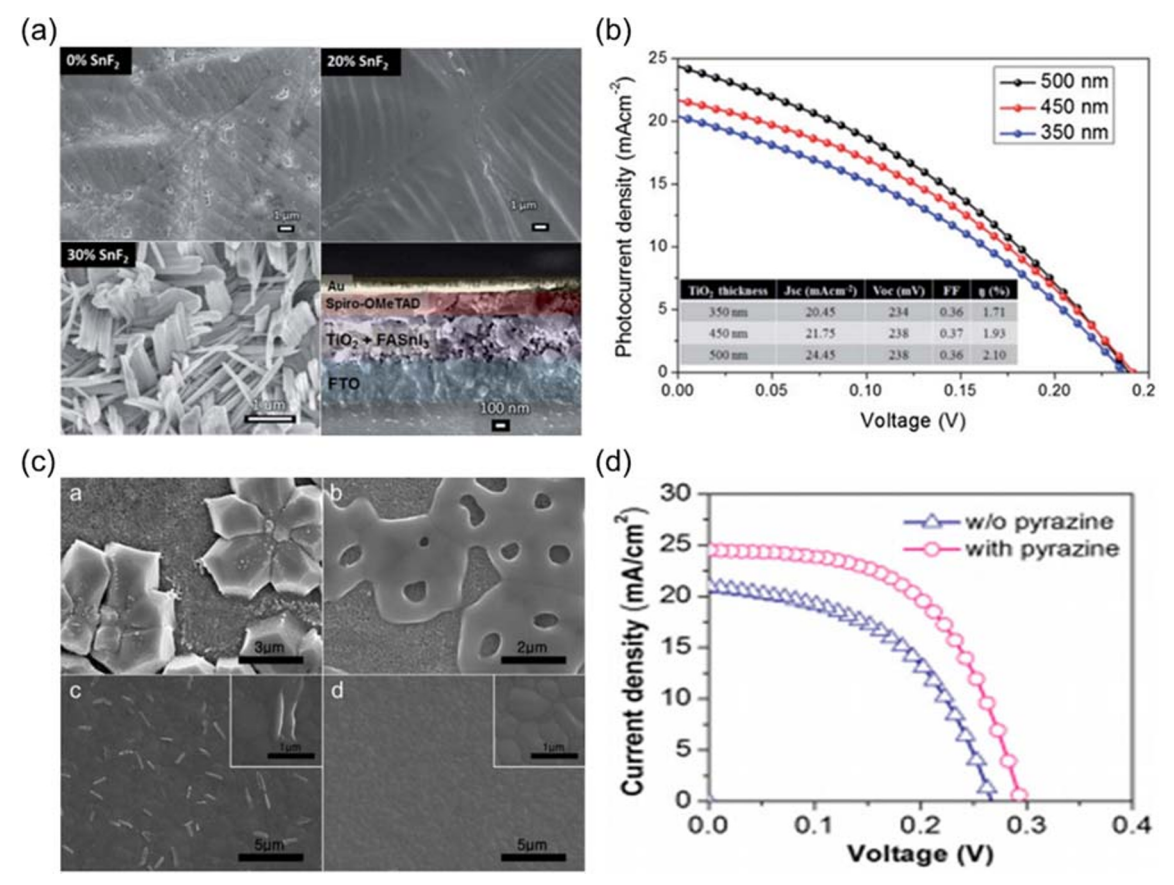


Fig. 7 a Top view FESEM (Field-emission Scanning Electron Microscope) images of FASnI₃ and FASnI₃:20%SnF₂ and FASnI₃:20%SnF₂ perovskite films deposited on the mp-TiO₂ layer and cross-sectional FESEM view of the full device. **b** J–V curves of FASnI₃:20%SnF₂ devices with different TiO₂ thicknesses. The inset shows the photovoltaic parameters of the respective devices. Reprinted with permission from ref. [91] Copyright 2015 American Chemical

Society. **c** Top view SEM images of FASnI₃ films fabricated using DMF solvent (*a*) without non-solvent dripping and (*b*) with non-solvent dripping and FASnI₃ films fabricated using mixed solvent of DMF and DMSO with non-solvent dripping (*c*) in the absence of pyrazine and (*d*) in the presence of pyrazine. **d** The J–V curves of FASnI₃ devices with and without pyrazine treatment. Reprinted with permission from ref. [92] Copyright 2016 American Chemical Society

boosted PCEs but also possessed suppressed photocurrent hysteresis. In 2019, Gong's group also reported efficient PSCs by Nd^{3+} partially substituted perovskites [35]. As indicated in Fig. 10d, MAPbI₃:xNd³⁺ (x = 0, 0.1, 0.5, 1.0, and 5.0 mol%) thin films possess both blue-shift absorption and PL spectra compared to pristine perovskites. XRD studies indicated that MAPbI₃:xNd³⁺ (x = 0, 0.1, 0.5, 1.0, and 5.0 mol%) thin films possessed superior crystallinity as compared with pristine perovskites, which was illustrated in Fig. 10e. The J–V characteristics of PSCs by either Nd³⁺ partially substituted perovskites or pristine perovskites are shown in Fig. 10f. PSCs by Nd³⁺ partially substituted perovskites exhibited a PCE of 21.15%, which was a 20% improvement compared to that by pristine perovskites.

4 The inorganic anion X⁻

It was also found that halide anion (Cl, Br, I) played an important role in the photovoltaic performance [109–111]. As









indicated in Fig. 11a, b, single crystalline MAPbX₃ (X = I, Br, Cl) exhibited different band gaps. For example, the band gaps of MAPbI₃, MAPbBr₃, and MAPbCl₃ are 1.53 eV, 2.24 eV, and 2.97 eV, respectively. Moreover, single crystalline MAPbBr₃ showed an electron mobility of 34 cm² V⁻¹ s⁻¹ and a hole mobility of 4.36 cm² V⁻¹ s⁻¹ [104, 112].

4.1 MAPbBr₃ perovskites

Hodes et al. reported PSCs by solution-processed MAPbBr₃ thin film, with a device architecture of FTO/c-TiO₂/mp-TiO₂/MAPbBr₃/organic hole transporting materials (HTM)/Au [113]. A $V_{\rm OC}$ of \sim 1.30 V was obtained from PSCs through tuning the valence bands of organic HTM. But PSCs exhibited poor PCEs.

Soek et al. reported PSCs by MAPbBr₃ thin film, with a device architecture of $ITO/mp-TiO_2/MAPbBr_3/HTM/Au$ [105]. As indicated in Fig. 11c, different HOMO levels of the HTM resulted in different $V_{\rm OC}$, from 1.29 V by using PTAA as the HTM to 1.36 V by using PF8-TAA as the

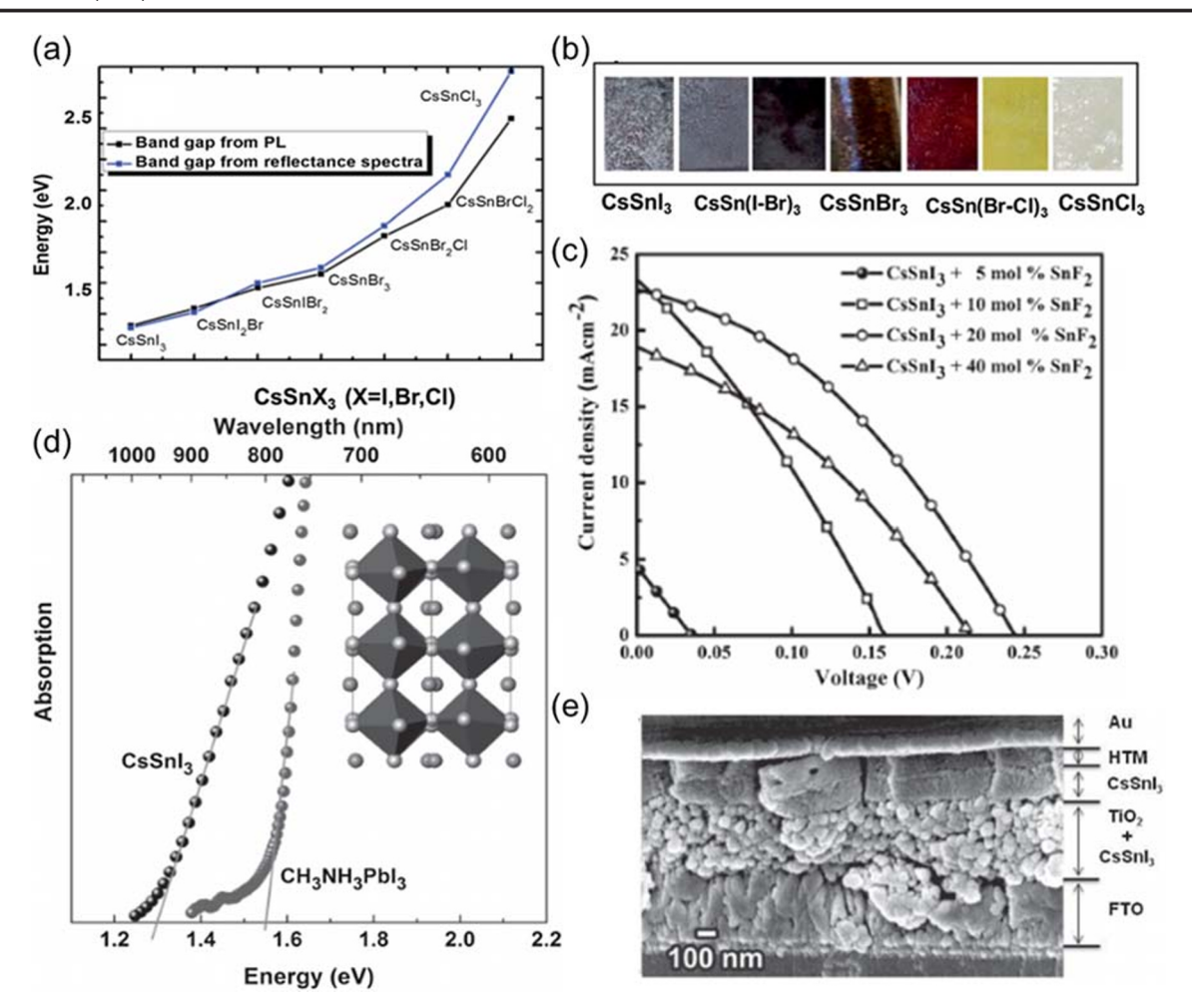


Fig. 8 a Band gap variation of different compositions estimated from absorption spectra and emission spectra for cesium tin halide perovskites. **b** Color variation of different compositions for cesium tin halide perovskites. Reprinted with permission from ref. [93] Copyright 2016 the Royal Society of Chemistry. **c** The J–V curves of photovoltaic

devices fabricated with different amounts of SnF₂. **d** Absorption spectra of CsSnI₃ and MAPbI₃. **e** The cross-sectional SEM image of the full device employing CsSnI₃ perovskite. Reprinted with permission from ref. [94] Copyright 2014 WILY-VCH

HTM, and then to 1.40 V by using PIF8-TAA as the HTM. The largest $V_{\rm OC}$ of 1.40 V and a moderate PCE of 6.7% were observed in Fig. 11d. In addition, 10% PCE was reported from PSCs by MAPbBr₃ thin film through controlling crystallization in the spin-coating process [114].

It was reported that high-quality MAPbBr₃ thin film could also be achieved by a vapor-assisted method [106]. In the vapor-assisted process, MAPbBr₃ thin film was deposited onto the mp-TiO₂ via spin-coating of precursor PbBr₂ solution firstly, and then PbBr₂ layer was treated with MABr vapor for 10 min, as shown in Fig. 11e. PSCs by MAPbBr₃ prepared by a vapor-assisted deposition method exhibited a $V_{\rm OC}$ of 1.45 eV, with a comparable PCE of 8.7%. As indicated in Fig. 11f, Wu et al. also reported a record-high- $V_{\rm OC}$ of 1.61 eV and a PCE of 7.5% from PSCs with a device architecture of ITO/PEDOT:PSS/MAPbBr₃/ICBA/Ca/Al [107].

4.2 MAPbCl_xl_{3-x} perovskites

As for CH₃NH₃PbI_{3-x}Cl_x perovskites, whether chlorine really involved into the perovskite crystals or not is still under investigation. Various explanations were described this fundamental question [115–117]. In 2014, Zhao and co-workers conducted the X-ray photoelectron spectroscopy (XPS) to measure the atomic percentage of chlorine in CH₃NH₃PbI_{3-x}Cl_x perovskite thin film and found out that only 1% chlorine within CH₃NH₃PbI_{3-x}Cl_x perovskite thin film [116]. Thus, it was assumed that chlorine atom might be removed during thermal annealing process of CH₃NH₃PbI_{3-x}Cl_x perovskite thin film. In order to verify this assumption, the energy dispersive X-ray (EDX) spectroscopy was carried out to obtain the atomic percentage of chlorine and other elements (Pb, I) from FTO/Perovskite and FTO/Perovskite/PMMA (blocking layer) thin films. It was found that both color and chlorine atomic









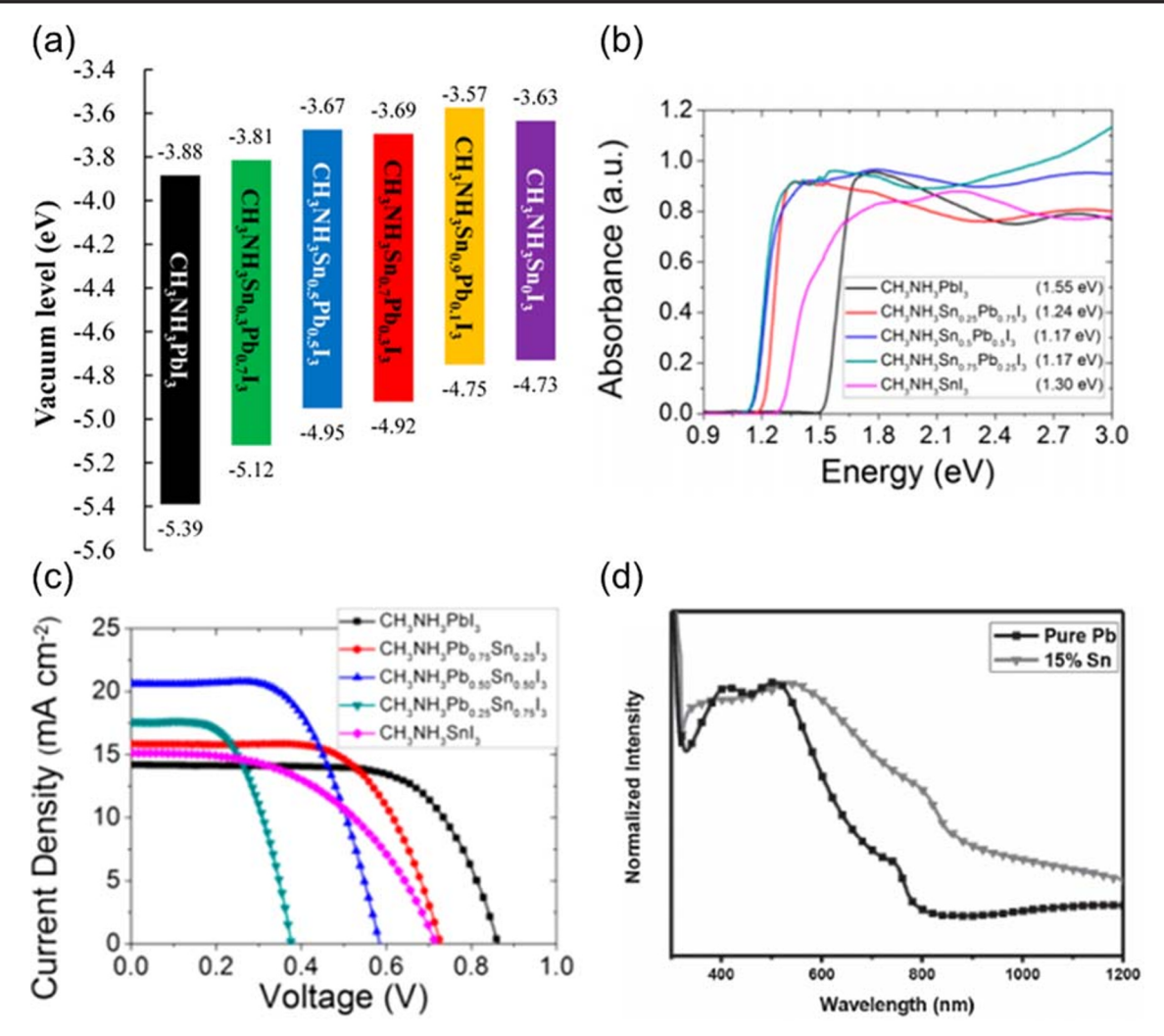


Fig. 9 a Schematic energy level diagram for $MASn_xPb_{1.x}I_3$ perovskites. Reprinted with permission from ref. [98] Copyright 2014 American Chemical Society. **b** Schematic energy level diagram and absorption spectrum for $MASn_xPb_{1.x}I_3$ perovskites. **c** The J–V curves of

photovoltaic devices with MASn_xPb_{1-x}I₃ perovskites. Reprinted with permission from ref. [99] Copyright 2014 American Chemical Society. **d** UV–Vis absorption spectrum of pure MAPbI₃ and MAPb_{0.85}Sn_{0.15}I₃. Reprinted with permission from ref. [100] Copyright 2014 WILY-VCH

percentage were changed after perovskite thin films were thermally annealed. The possible reactions during the annealing processes were proposed as follows:

- (1) $PbCl_2 + 3CH_3NH_3I \rightarrow PbI_2 + CH_3NH_3I + 2CH_3NH_3Cl$;
- (2) $PbI_2 + CH_3NH_3I + 2CH_3NH_3Cl \rightarrow CH_3NH_3PbI_3 + 2CH_3NH_3Cl(g);$
- (3) $PbI_2 + xCH_3NH_3I + yCH_3NH_3Cl \rightarrow (CH_3NH_3)_{x+y}PbI_{2+y}$ $_xCl_y$ (Intermediate phase) $\rightarrow CH_3NH_3PbI_3 + CH_3NH_3Cl$ (g).

Thus, it was concluded that CH₃NH₃⁺ is essential to retard the growth of perovskite crystals. In addition, through the utilization of transmission electron microscopy (TEM), Jen's group observed enhanced charge carrier lifetime and diffusion length assisted by the presence of chlorine component [115].

Snaith et al. reported the electron-hole diffusion lengths and lifetimes in MAPbI₃ and MAPbCl_xI_{3-x} perovskites [118]. It was found that MAPbI₃ has an electron-hole

diffusion length of ~ 100 nm, whereas the electron-hole diffusion length in MAPbCl_xI_{3-x} was nearly 1 μ m. Such large diffusion length certainly could benefit charge generation and collection since non-radiative electron-hole recombination was suppressed [119, 120]. Thus, it was stated that chlorine-based perovskites play a significant role in the film morphology evolution of MAPbCl_xI_{3-x} perovskites [115]. Yang et al. also reported the role of chlorine in MAPbCl_xI_{3-x} perovskites [117]. It was also found that efficient electron-hole transport across the interfaces between bulk perovskite layer and charge carrier transport layer was boosted [117].

4.3 MAPbBr_xI_{3-x} perovskites

Studies indicated that the presence of bromine component within CH₃NH₃PbI_{3-x}Br_x perovskites has three contributions [108, 121–124]: (1) to improve the stability of CH₃NH₃PbI_{3-x}Br_x perovskites, (2) to increase charge









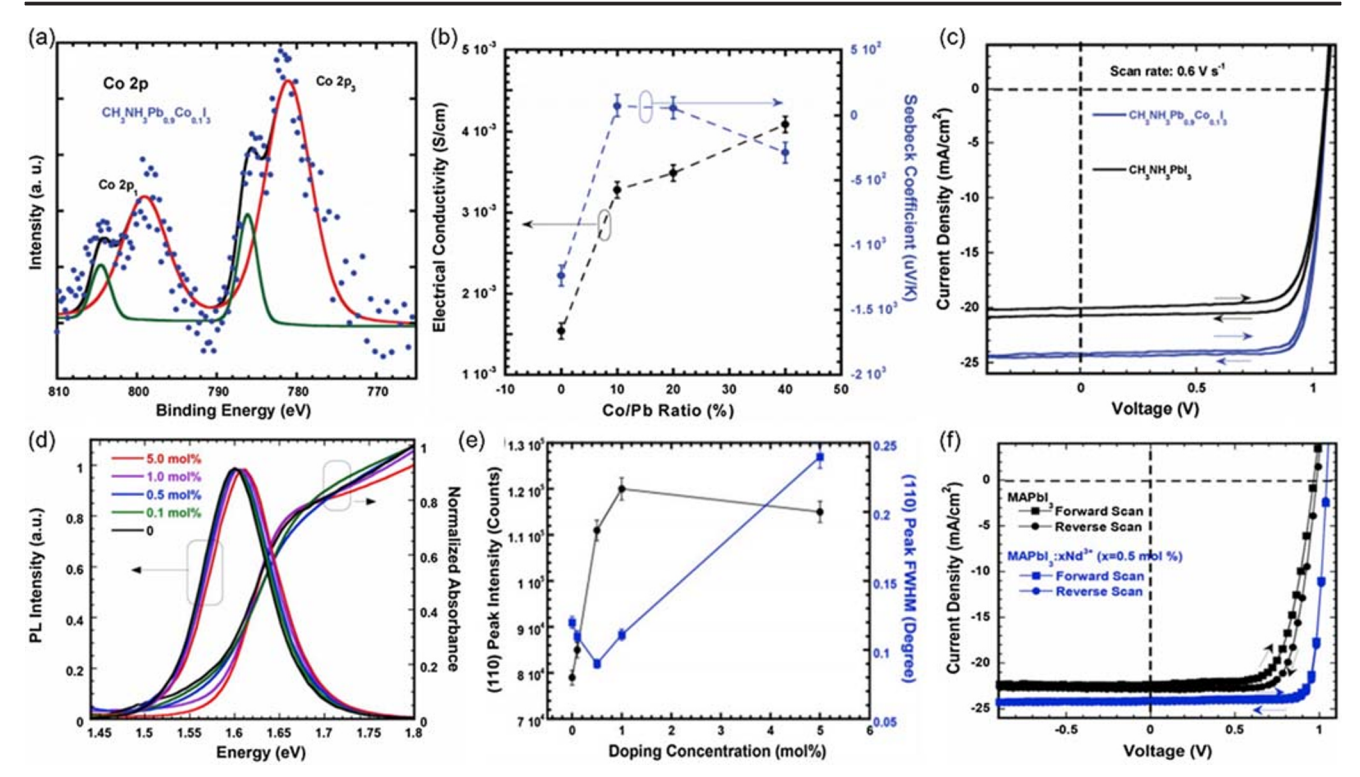


Fig. 10 a The XPS spectra of Co 2p from the MAPb_{0.9}Co_{0.1}I₃ thin film. **b** The electrical conductivities and the Seebeck coefficients of the MAPb_{1.x}Co_xI₃ (x=0,0.1,0.2, and 0.4) thin films. **c** The J–V characteristics of the pristine device and Co-substituted device. Reprinted with permission from ref. [36] Copyright 2018 WILY-VCH. **d** The steady-state PL spectra and absorption spectra of CH₃NH₃PbI₃:xNd³⁺ (x=0,0.1,0.5,1.0, and

5.0 mol%) thin films. **e** The (110) peak intensity and the FWHM (Full width at half maximum) variations calculated from XRD spectra for the $CH_3NH_3PbI_3:xNd^{3+}$ (x=0,0.1,0.5,1.0, and 5.0 mol%) thin films. **f** The J–V characteristics of the pristine device and Nd-doped device. Reprinted with permission from ref. [35] Copyright 2019 Elsevier

carrier mobility and suppress charge carrier recombination, and (3) to enlarge $V_{\rm OC}$ due to the increased band gap along with increased Br⁻ concentrations.

It was found that the band gaps of MAPbBr_xI_{3-x} can be linearly tuned from 1.58 to 2.28 eV as x was changed from 0 and 1, as indicated in Fig. 11g [108]. Seok et al. reported PSCs by MAPbBr_{0.6}I_{2.4} thin film exhibiting a PCE of 12.3% and a $V_{\rm OC}$ of 0.91 V [108]. Etgar et al. reported the HTL-free PSCs by MAPbBr_xI_{3-x} exhibiting a PCE of 8.5%, a $J_{\rm SC}$ of 16 mA cm⁻², with improved stability [125].

4.4 MAPbBr_xCl_{3-x} perovskites

It was reported that PSCs by MAPbBr_xCl_{3-x} exhibited a $V_{\rm OC}$ of 1.5 V, a $J_{\rm SC}$ of 4 mA cm⁻², and a PCE of 2.0% [126]. It was also found that additional lead chloride can improve the photovoltaic performance of PSCs by MAPbBr_xCl_{3-x} via controlling the formation of perovskite thin film [127]. These studies indicated that the slower dissolution of lead chloride in DMF could induce emergence of lead chloride particles, providing a heterogeneous nucleation sites for the crystallization of perovskite [127].

5 Other hybrid perovskite materials

Lead-free perovskites, lead-free 2D perovskites, and perovskites co-crystalized with polymers were also investigated for boosting device performance of PSCs.

5.1 Less-toxic perovskites

Efficient PSCs by lead-based perovskites have been reported, but the toxicity of lead was a challenge. Such difficulty has motivated scientists to look for perovskites with no and less toxicity [39, 132, 133]. A₃Bi₂I₉, one of perovskites, was stood out since Bi³⁺ has the outer lone pair of 6s² electron, which plays a key role in the optoelectronic properties of the resultant perovskites [134, 135]. A₃Bi₂I₉ adopts a face-sharing or non-punctual dioctahedral (Bi₂I₉)³⁻ clusters, as shown in Fig. 12a [136]. Johansson et al. reported both Cs₃Bi₂I₉ and MA₃Bi₂I₉ thin films prepared by spin-coating of a precursor solution composing of CsI mixed with BiI₃, MAI, and BiI₃, and then followed with thermal annealing at low temperature [128]. The band gap of Cs₃Bi₂I₉ was 2.2 eV, whereas the band gap of MA₃Bi₂I₉ was 2.1 eV, as indicated in Fig. 12b. It was also found that the Wannier–Mott binding energies for Cs₃Bi₂I₉









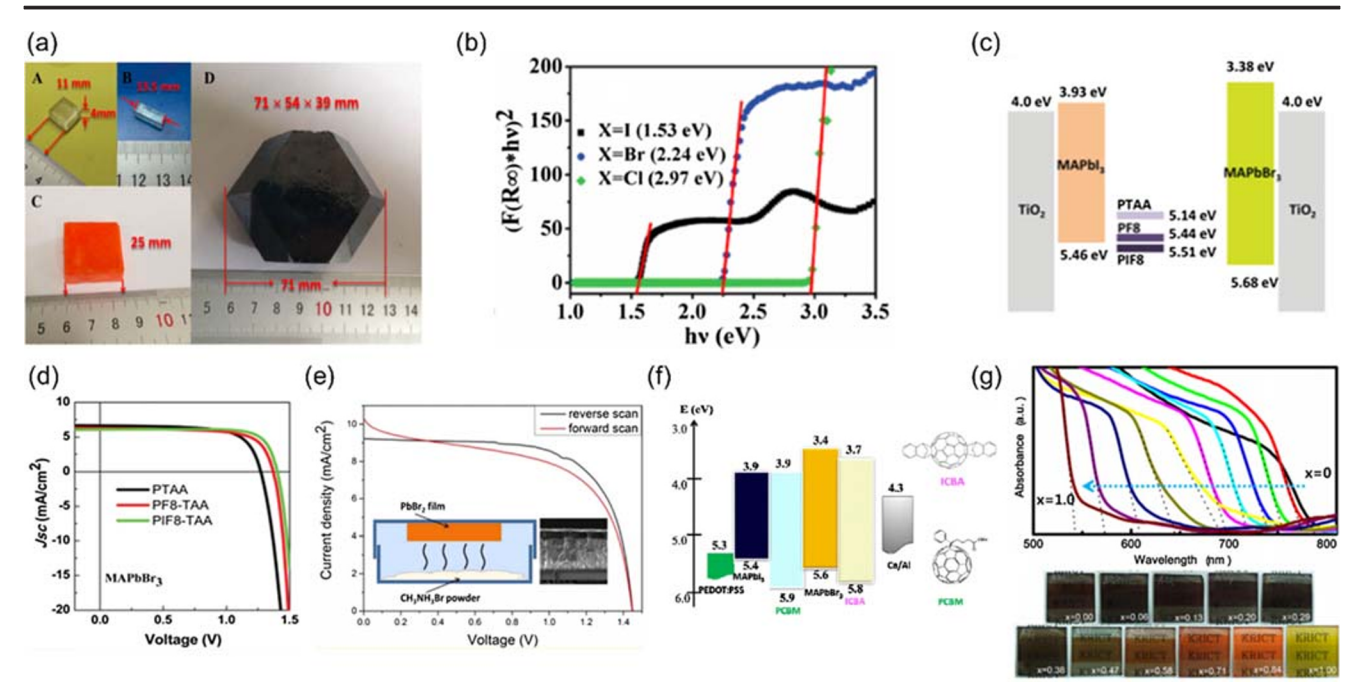


Fig. 11 a Photograph for MAPbX₃ single crystals (A, B) X = Cl, (C) X = Br, (D) X = I. **b** The band gap of MAPbX₃ single crystals. Reprinted with permission from ref. [104] Copyright 2015 WILY-VCH. **c** Schematic energy band level diagrams for TiO₂, MAPbI₃, and MAPbBr₃ perovskites, and PTAA, PF8-TAA, and PIF8-TAA. **d** The J–V curves of the device with different HTMs (PTAA, PF8-TAA, PIF8-TAA). Reprinted with permission from ref. [105] Copyright 2016 the Royal Society of Chemistry. **e** The J–V curves of MAPbBr₃ perovskite solar cell via vapor-assisted deposition and inset image for schematic

illustration of vapor-assisted deposition process. Reprinted with permission from ref. [106] Copyright 2013 American Chemical Society. **f** Schematic energy band level diagrams for PEDOT:PSS, MAPbBr₃ perovskites, and ETMs (ICBA, PCBM, Ca/Al). Reprinted with permission from ref. [107] Copyright 2014 the Royal Society of Chemistry. **g** UV–Vis absorption spectrum and photographs of different compositions for MAPb(I_{1-x}Br_x)₃ perovskites. Reprinted with permission from ref. [108] Copyright 2015 American Chemical Society

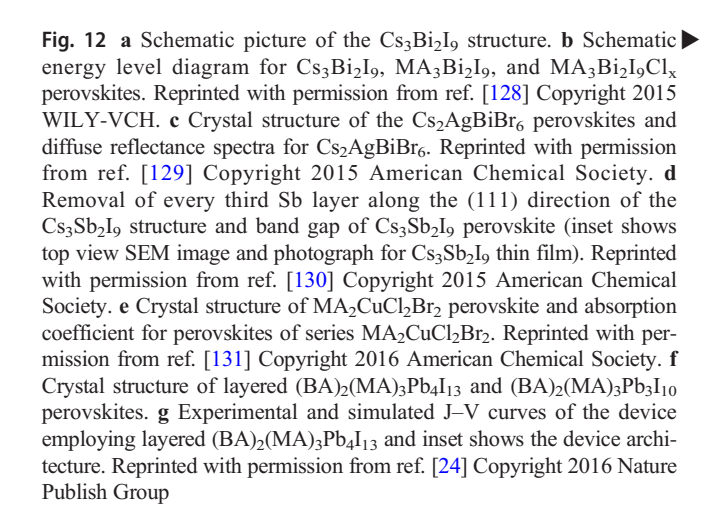
and MA₃Bi₂I₉ were 70 and 270 meV, respectively [137]. PSCs by either Cs₃Bi₂I₉ or MA₃Bi₂I₉ thin films exhibited PCEs of 1.09% and 0.12%, respectively. However, the stabilities of above PSCs were poor [137, 138].

Cs₂AgBiBr₆ and Cs₂AgBiCl₆ were also reported [139]. Both Cs₂AgBiBr₆ and Cs₂AgBiCl₆ were with cubic double perovskite structures and they were indirect band gap semiconductors, as shown in Fig. 12c [140]. The band gaps of Cs₂AgBiBr₆ and Cs₂AgBiCl₆ were found to be 2.19 and 2.77 eV, respectively. The double perovskites have a big family, but was less studied in their optoelectronic properties [129, 130, 141]. Cs₃Sb₂I₉ thin film treated by layered modification exhibited a band gap of 2.05 eV, as illustrated in Fig. 12d. But PSCs by Cs₃Sb₂I₉ thin film displayed a poor photovoltaic performance, which might be attributed to the presence of deep level defects.

5.2 2D perovskites

In general, the dramatically difference between the RP phase and the DJ phase within 2D perovskites was utilization of different types of organic spacer [142]. In the RP phase 2D perovskites, the organic spacer was the monovalent cation while the organic spacer was the divalent cation in the DJ phase 2D perovskites. In the RP phase, the

monovalent cation can only form hydrogen bonds with one-side inorganic perovskite sheets. Thus, there is a very weak van-der-Waals gap between the adjacent organic spacers. However, in the DJ phase, the divalent cation can form hydrogen bonds with both-side inorganic layers without any gaps, resulting in stable 2D perovskite structure.











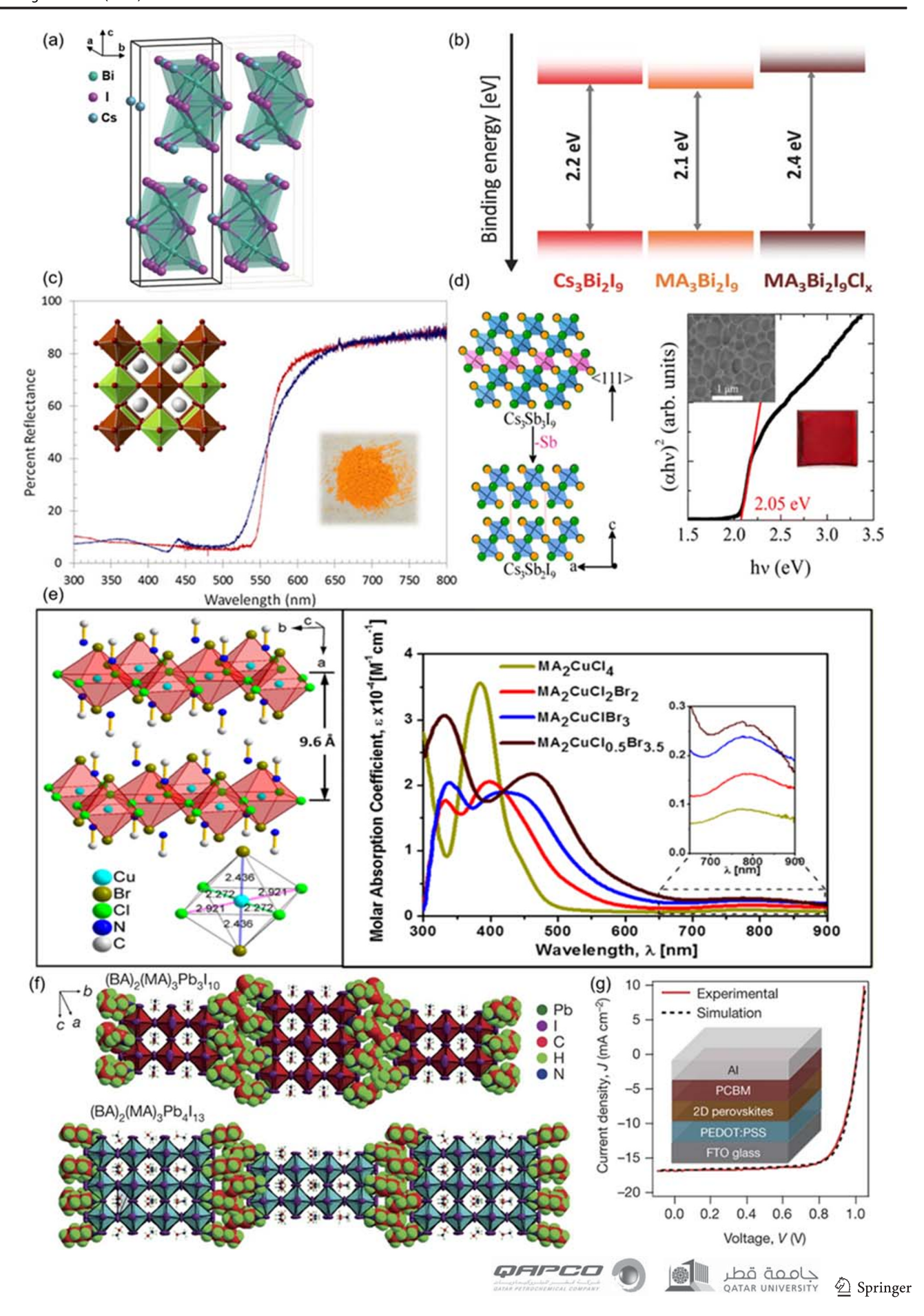


 Table 1
 Summary of information of various compositional perovskite materials

I CLOVSKIICS	$E_{\rm g}$ (eV)	Device architecture	$V_{\rm oc}(V)$	$J_{\rm SC}$ (mA cm z)	FF (%)	PCE (%)	Synthetic method	Ref
FAPbI ₃	1.47	FTO/bl/mp-TiO ₂ /Perovskite/Spiro/Au	0.97	6.5	69	4.3	Sequential deposition	[50]
$FAPbI_3$		FTO/bl/mp-TiO ₂ /Perovskite/P3HT/Au	0.84	18.3	50	7.5	In situ dipping technique	[51]
$FAPbIBr_2$	1.48	FTO/bl-TiO2/Perovskite/Spiro/Au	0.94	23.3	65	14.2	Adding hydroiodic acid to the FAI:PbI ₂ (1:1)	[53]
$(FAPbI_3)_{0.85}(FAPbBr_3)_{0.15}$	1.49	FTO/NiO/Perovskite/PCBM/LiF/Al	1.06	24.7	78	20.2	Intramolecular exchange process	[52]
$FAPbBr_3$	2.26	FTO/bl-TiO ₂ /Perovskite/Spiro/Au	1.35	9.9	73	6.5	Two-step deposition	[4] [4]
FAPbI ₃		FTO/bl/mp-TiO2/Perovskite/Spiro/Ag	1.04	22.3	75	18.1	Organic cation displacement	[145]
FAPbI ₃		FTO/bl-TiO ₂ /Perovskite/Spiro/Au	1.03	20.9	99	14.2	Chemical vapor deposition (CVD)	[146]
FAPbI ₃		FTO/bl-TiO ₂ /Perovskite/Spiro/Ag	1.11	21.4	70	16.6	Controlled humidity	[147]
$FAPbI_xCI_{3-x}$	1.49	FTO/bl/mp-TiO ₂ /Perovskite/P3HT/Au	0.65	20.0	51	9.9	One-step deposition	[148]
CsPbI ₃	1.73	FTO/bl/mp-TiO ₂ /Perovskite/Spiro/Au	08.0	12.0	30	2.9	Adding hydroiodic acid to the CsI:PbI ₂ (1:1)	[55]
$CsPbBr_3$	2.36	FTO/bl/mp-TiO2/Perovskite/PTAA/Au	1.28	6.2	74	5.9	Sequential deposition	[99]
$CsPbIBr_2$	2.05	FTO/bl-TiO ₂ /Perovskite/Au	0.95	8.7	99	4.7	Dual source thermal evaporation	[57]
$CsPbI_3$		FTO/bl/mp-TiO ₂ /Perovskite/P3HT/MoO ₃ /Au	0.58	8.9	50	2.0	One-step deposition	[149]
$\mathrm{FA}_{0.4}\mathrm{MA}_{0.6}\mathrm{PbI}_{3}$		FTO/bl/mp-TiO2/Perovskite/Spiro/Au	1.00	21.2	70	14.9	Sequential deposition	[63]
$\mathrm{FA}_{0.4}\mathrm{MA}_{0.6}\mathrm{PbI}_{3}$		ITO/PEDOT:PSS/Perovskite/PCBM/Ca/Al	0.94	18.9	73	13.0	The formation of (FAI) _{1-x} -PbI ₂ intermediate	[64]
$(FAPbI_3)_{0.85}(MAPbBr_3)_{0.15}$		FTO/bl/mp-TiO2/Perovskite/PTAA/Au	1.11	22.5	73	18.4	One-step deposition	[65]
$(FAPbI_3)_{1-x}(MAPbBr_3)_x$		FTO/bl/mp-TiO2/Perovskite/Spiro/Au	1.16	24.6	73	20.8	One-step deposition and anti-solvent assistant	[99]
$\mathrm{Cs}_{0.1}\mathrm{MA}_{0.9}\mathrm{PbI}_3$	1.52	ITO/PEDOT:PSS/Perovskite/PCBM/Al	1.05	10.1	73	7.6	One-step deposition	[29]
$\mathrm{Cs}_{0.1}\mathrm{FA}_{0.9}\mathrm{PbI}_{3}$		FTO/bl-TiO ₂ /Perovskite/Spiro/Ag	1.02	23.0	64	19.0	Using DMSO adduct of PbI ₂	[89]
${ m Cs_{0.2}FA_{0.8}Pbl_{2.84}Br_{0.16}}$	1.58	FTO/bl/mp-TiO2/Perovskite/Spiro/Au	1.07	23.3	72	18.0	One-step deposition and anti-solvent assistant	[69]
$\mathrm{Cs}_{0.15}\mathrm{FA}_{0.85}\mathrm{PbI}_{3}$		FTO/bl/mp-TiO2/Perovskite/Spiro/Au	1.08	21.5	75	17.3	One-step deposition and anti-solvent assistant	[150]
$MASnI_3$	1.30	FTO/bl-TiO ₂ /Perovskite/Spiro/Au	89.0	16.6	48	5.2	One-step deposition	[82]
$MASnI_3$		FTO/bl/mp-TiO2/Perovskite/Spiro/Au	0.88	16.8	42	6.4	One-step deposition	[06]
$MASnI_3$		FTO/bl/mp-TiO2/Perovskite/Au	0.32	21.4	46	3.2	Using DMSO adduct of SnI ₂	[83]
$FASnI_3$	1.41	FTO/bl/mp-TiO2/Perovskite/Spiro/Au	0.23	24.4	36	2.1	Precursor solution incorporating 20 mol% of SnF_2	[91]
$FASnI_3$		FTO/bl/mp-TiO2/Perovskite/Spiro/Au	0.29	24.5	55	4.0	Additional pyrazine dripping process	[95]
CsSnI ₃	1.31	FTO/bl/mp-TiO2/Perovskite/m-MTDATA/Au	0.24	22.7	37	2.0	Incorporating 20 mol% of SnF ₂	[94]
$\mathrm{MASn}_{0.5}\mathrm{Pb}_{0.5}\mathrm{I}_{3}$	1.28	FTO/bl/mp-TiO2/Perovskite/P3HT/Au	0.42	20.0	50	4.2	One-step deposition	[86]
$\mathrm{MASn}_{0.5}\mathrm{Pb}_{0.5}\mathrm{I}_{3}$		FTO/bl/mp-TiO2/Perovskite/Spiro/Au	0.58	20.3	09	7.3	Adding HI/H ₃ PO ₂ to the precursor solution	[66]
$MAPb_{0.85}Sn_{0.15}I_xCI_{3-x}$		ITO/PEDOT:PSS/Perovskite/PCBM/Bis-C ₆₀ /Ag	0.79	19.1	99	6.7	One-step deposition	[100]
$MAPbBr_3$	2.32	FTO/bl/mp-TiO2/Perovskite/PDI/Au	1.30	1.0	40	0.5	One-step deposition	[113]
$MAPbBr_3$		FTO/bl/mp-TiO2/Perovskite/PIF8-TAA/Au	1.40	6.1	70	6.7	One-step deposition	[105]
$MAPbBr_3$		FTO/bl/mp-TiO ₂ /Perovskite/PIF8-TAA/Au	1.51	8.4	82	10.4	The addition of HBr in precursor solution	[114]
$MAPbBr_3$		FTO/bl/mp-TiO ₂ /Perovskite/Spiro/Au	1.45	9.5	62	8.7	Vapor-assisted deposition	[106]
$MAPbBr_3$		ITO/PEDOT:PSS/Perovskite/ICBA/Ca/Al	1.61	0.9	77	7.5	Sequential deposition with solvent annealing	[107]











ned
ontir
<u> </u>
$\overline{}$
le
3
ಡ

Perovskites	$E_{\rm g} \left({ m eV} \right)$	$E_{\rm g}$ (eV) Device architecture	$V_{\rm OC}\left({ m V}\right)$	$J_{\rm SC}~({\rm mA~cm}^{-2})$	FF (%)	PCE (%)	$V_{\rm OC}$ (V) $J_{\rm SC}$ (mA cm ⁻²) FF (%) PCE (%) Synthetic method	Ref
$MAPbCl_xI_{3-x}$		FTO/bl-TiO ₂ /Perovskite/Spiro/Au	1.02	21.0	75	16.1	Sequential deposition	[117]
$MAPbI_2Br$		FTO/bl-TiO2/TiO2NWAs/Perovskite/Spiro/Au	0.82	10.1	59	4.8	One-step deposition	[126]
$MAPbl_{2.4}Br_{0.6}$	1.66	FTO/bl/mp-TiO ₂ /Perovskite/PTAA/Au	0.91	19.3	70	12.3	One-step deposition	[108]
MAPbBr _x Cl _{3-x}		FTO/bl/mp-TiO ₂ /Perovskite/Spiro/Au	1.24	7.8	99	5.4	One-step deposition	[135]
$MAPbBr_xCl_{3-x}$	2.30	FTO/bl/mp-TiO ₂ /Perovskite/CBP/Au	1.50	4.0	40	2.7	One-step deposition	[127]

 Table 2
 Device performance parameters of PSCs by either the RP or the DJ 2D perovskites

T CLOV SIKINGS	$E_{\rm g}\left({ m eV}\right)$	$E_{\rm g}$ (eV) Device architecture	$V_{\rm oc}\left({ m V}\right)$	$V_{\rm OC} \left({ m V} \right) - J_{ m SC} \left({ m mA cm}^{-2} \right)$	FF (%)	PCE (%)	Synthetic method	Ref
$(GA)(MA)_3Pb_3I_{10}$	1.61	FTO/c-TiO ₂ /Perovskite/PCBM/Ag	1.14	22.3	73	18.5	One-step deposition and anti-solvent assistant	[151]
$(3BBA)_{1.8}(MA)_{2.5}Pb_3(I_{1-x}CI_x)_{1.3}$	1.57	ITO/PTAA/Perovskite/PCBM/Cr/Au	1.23	18.2	81	18.2	One-step deposition and hot-casting method	[152]
$(4FPEA)_2MA_4Pb_5I_16$	1.62	ITO/PTAA/Perovskite/PCBM/Ag	1.16	19.0	79	17.3	One-step deposition and additive assistant	[153]
$(ThMA)_2(MA)_2Pb_3I_{10}$	1.59	ITO/PEDOT:PSS/Perovskite/PCBM/BCP/Ag	1.07	18.9	92	15.4	One-step deposition and anti-solvent assistant	[154]
$(PDA)MA_3Pb_4I_{13}$	1.69	FTO/TiO ₂ /Perovskite/Spiro/Au	86.0	19.5	69	13.3	One-step deposition and hot-casting method	[143]
$(BDA)MA_3Pb_4I_{13}$	1.88	ITO/PEDOT:PSS/Perovskite/PCBM/BCP/Ag	1.15	14.5	77	12.8	One-step deposition and additive assistant	[155]
$(BA)_2MA_3Pb_4I_{13}$	1.66	FTO/PEDOT:PSS/Perovskite/PCBM/Al	1.01	16.8	74	12.5	One-step deposition and hot-casting method	[54]
$(EA)_2(MA)_5Pb_6I_{19}$	1.61	ITO/C ₆₀ /Perovskite/Carbon	1.02	21.1	55	11.9	One-step deposition and anti-solvent assistant	[156]
$(PEA)_2MA_4Pb_5I_{16}$	1.65	ITO/PEDOT:PSS/Perovskite/PCBM/BCP/Ag	1.11	15.0	29	11.0	One-step deposition and additive assistant	[157]
$(iso-BA)_2(MA)_3Pb_4I_{13}$	1.74	FTO/C ₆₀ /Perovskite/Spiro/Au	1.20	16.5	53	10.6	One-step deposition and hot-casting method	[158]
$(PA)_2(MA)_4Pb_5I_{16}$	1.63	FTO/c-TiO ₂ /Perovskite/Spiro/Au	1.11	18.9	50	10.4	One-step deposition and hot-casting method	[159]
$(\mathrm{PEI})_2(\mathrm{MA})_6\mathrm{Pb}_7\mathrm{I}_{22}$	1.62	ITO/PEDOT:PSS/Perovskite/PCBM/LiF/Ag	1.10	13.1	65	10.1	One-step deposition	[160]
$(MeO-PEA)_2MA_4Pb_5I_{16}$	1.59	ITO/PEDOT:PSS/Perovskite/PCBM/BCP/Ag	1.10	12.0	71	9.4	One-step deposition	[161]
$(Anyl)_2(MA)_4Pb_5I_{16}$	1.59	FTO/c-TiO ₂ /Perovskite/Spiro/Au	0.82	13.8	89	7.6	One-step deposition and hot-casting method	[162]
$(C(NH_2)_3)_2(CH_3NH_3)_3Pb_3I_{10}$	1.73	FTO/PEDOT:PSS/Perovskite/PCBM/Al	0.97	9.4	80	7.3	One-step deposition and anti-solvent assistant	[163]
$(3AMP)(MA)_3Pb_4I_{13}$	1.92	FTO/PEDOT:PSS/Perovskite/C60/BCP/Ag	1.06	10.2	69	7.3	One-step deposition and anti-solvent assistant	[25]
$(HdA)_2PbI_4$	2.44	FTO/c-TiO ₂ /mp-TiO ₂ /Perovskite/Spiro/Ag	0.72	1.7	47	9.0	Single crystal method	[164]











The compositional engineering on lead-based 2D perovskite materials was overviewed in our recently publication [39] and others [40, 41]. Here, we highlight other 2D perovskites.

It was found that MA₂CuCl_{4-x}Br_x perovskites possess a 2D layered structure, which is similar to the Ruddlesden–Popper phase structure like K₂NiF₄. The smaller ionic radius of Cu⁺ cation hinders 3D arrangement in MA₂CuCl_{4-x}Br_x perovskites [131]. The absorption onset of MA₂CuCl_{4-x}Br_x perovskites can be tuned from 500 nm for MA₂CuCl₄ to 689 nm for MA₂CuCl_{0.5}Br_{3.5} by the variation of Br⁻ component, which was attributed to the ligand-to-metal charge transition, as demonstrated in Fig. 12e. The additional absorption in MA₂CuCl_{4-x}Br_x perovskites can be extended up to 700 nm or 900 nm. PSCs by either MA₂CuCl₄ or MA₂CuCl_{0.5}Br_{3.5} incorporated with mp-TiO₂ as the ETL and spiro-MeOTAD as the HTL exhibited PCEs of 0.017% or 0.0017%, respectively [131].

Another Ruddlesden–Popper phase, layered 2D perovskites, as shown in Fig. 12f, PSCs exhibited a remarkably PCE of 12.5% with no photocurrent hysteresis [24]. It was found that $(BA)_2(MA)_3Pb_4I_{13}$ thin films possess superior crystallinity and uniformity. PSCs by $(BA)_2(MA)_3Pb_4I_{13}$ thin films displayed a PCE of 12.51%, a $V_{\rm OC}$ of 1.01 V, a $J_{\rm SC}$ of 17.76 mA cm⁻², and an FF of 74.13%, as shown in Fig. 12g. In addition, PSCs by $(BA)_2(MA)_3Pb_4I_{13}$ thin films showed a long-term stability.

In 2019, Li's group observed the DJ phase through conducting a hot-casting strategy and further optimized the device performance [143]. It was found at the hot-casting temperature of 190°C, perovskite thin film could achieve large grain size and good orientation. PSCs by (PDA)(MA)₃Pb₄I₁₃ perovskites (PDA, 1,3-propanediamine) exhibited $V_{\rm OC}$ = 0.98 V, $J_{\rm SC}$ = 19.5 mA/cm², and FF = 69%, with a corresponding PCE of 13.3%, and good stability [143].

The device performance parameters of PSCs by either the RP or the DJ 2D perovskites are summarized in Tables 1 and 2.

5.3 Perovskites co-crystalized with polymers

A novel kind of perovskites co-crystalized with polymers has been recently reported by Gong's group [165, 166]. It was found that poly(ethylene oxide) (PEO) can form hydrogen bonds with MAPbI₃ perovskites, which was shown in Fig. 13a [165]. As indicated in Fig. 13b, PSCs by perovskites co-crystalized PEO exhibited free photocurrent hysteresis. Moreover, as indicated in Fig. 13c, PSCs by perovskites co-crystalized PEO possessed much faster photocurrent response, which indicated the ion/vacancy migration and trap-filling were dramatically suppressed.

More recently, Gong's group reported perovskites cocrystalized polymers prepared by one-step self-assembled method [166]. As indicated in Fig. 13d, a weak "O-H" stretching vibration at $\sim 3500 \text{ cm}^{-1}$ and a sharp "C-H"









stretching vibration at $\sim 2880~\rm cm^{-1}$ were observed from perovskites co-crystalized PEO. Figure 13e displays the J–V characteristics of PSCs by pristine perovskites and perovskites co-crystalized PEO. PSCs by perovskites co-crystalized PEO exhibited a $J_{\rm SC}$ of 23.01 mA cm⁻², a $V_{\rm OC}$ of 1.12 V, a FF of 0.81, and a PCE of 20.78%, which was $\sim 20\%$ enhancement compared to that by pristine perovskites. As indicated in Fig. 13f, the photo response of PSCs by perovskites co-crystalized PEO was faster compared to that by pristine perovskites, indicating perovskites co-crystalized PEO thin film have less defects and trapstates

6 Conclusion and outlook

In summary, we have discussed compositional engineering of organic–inorganic hybrid perovskites and their optoelectronic and photovoltaic properties. Studies indicated that the compositional engineering of organic–inorganic hybrid perovskites plays an important role in tuning optoelectronic and photovoltaic properties of perovskites.

The introduction of FA⁺ organic cation into perovskites has been demonstrated to be a simple method in enhancement of PCEs of PSCs. Moreover, PSCs by Cs_xFA_{1-x}PbI₃ with longterm stability of 1000 h in the ambient condition have been reported. On the other hand, it has been demonstrated that varying the Sn:Pb ratios could tune the optoelectronic properties of the resultant perovskites. Perovskites containing metal cations, such as Cu²⁺, Ge²⁺, and Fe²⁺, have been developed and PSCs by these novel perovskites need to be optimized. For inorganic halide cation, bromine-containing perovskites showed a record $V_{\rm OC}$ of 1.61 V, which provided a potential application for electrochemical reactions, new tandem device architecture. The utility of mixed halide perovskite (MAPbCl_xI_{3-x}) has been used to improve charge carrier generation and collection, film morphology and reduce nonradiative electron-hole recombination. Finally, PSCs by Ruddlesden-Popper phase 2D layered perovskites exhibited a remarkable PCE of 12.5% and enhanced light and moisture stability have been demonstrated.

As we described that compositional engineering of perovskites could improve the stability, and eliminate the toxicity of perovskite materials. In order to generate perovskites with good stability and less/or no toxicity, substation of toxic Pb element by other cations and co-crystallization with polymers are ongoing directions.

Regarding cost-effective manufacturing of PSCs, it is believed that compositional engineering would also play an important role to meet various requirements on fabrication largearea PSCs. However, the origin of the light soaking and photocurrent hysteresis phenomena, defect-induced electron-hole

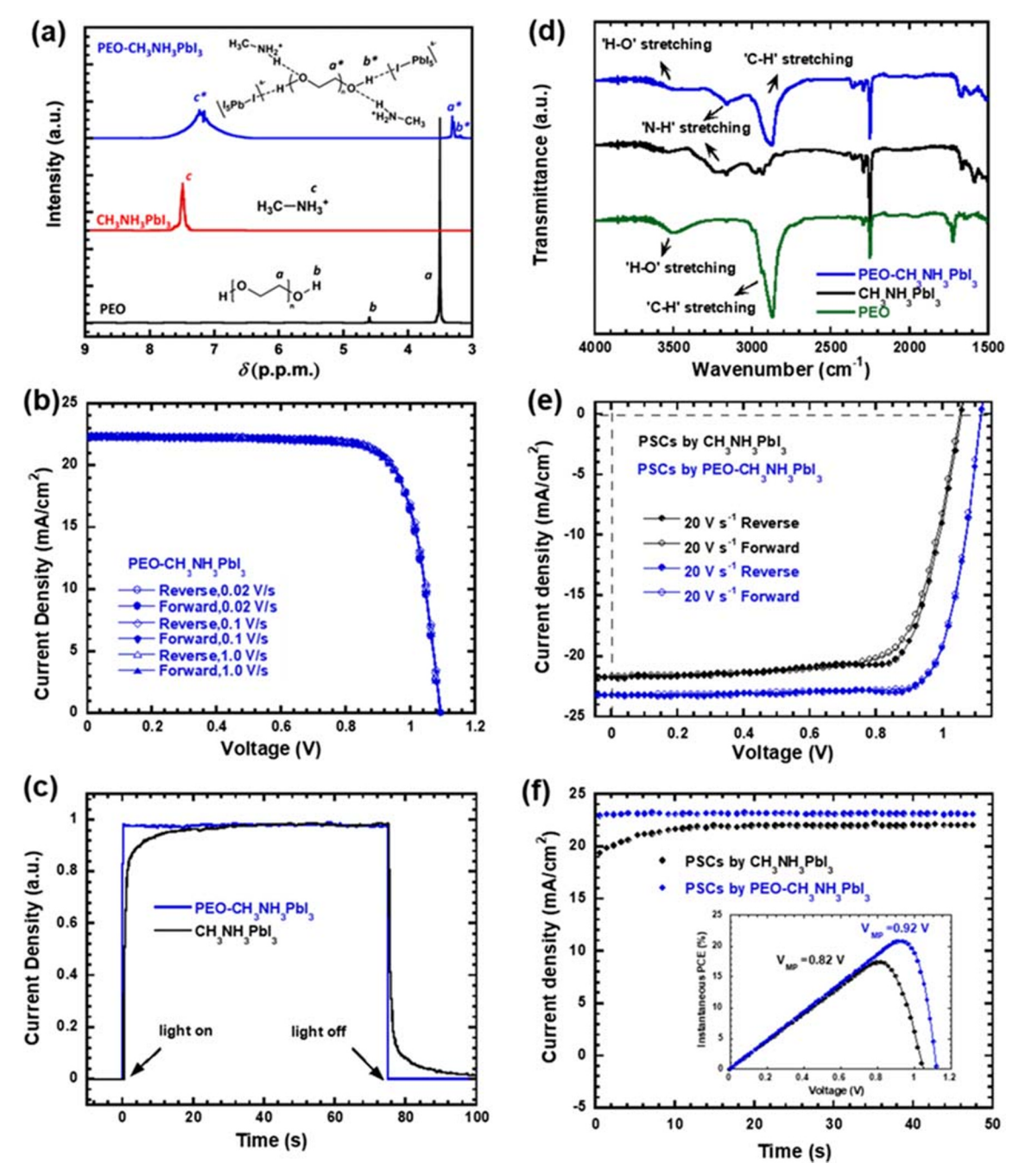


Fig. 13 a The NMR spectra for PEO, MAPbI₃, and PEO-MAPbI₃ solutions. **b** The J-V characteristics of devices by PEO-MAPbI₃ thin film under different scan directions and different scan rates. **c** The photocurrent rising process of devices under light-on and light-off conditions. Reprinted with permission from ref. [165] Copyright 2020 Elsevier. **d**

The FTIR spectra of MAPbI₃, PEO, and PEO-MAPbI₃ solutions. **e** The J–V characteristics of the pristine device and the PEO-doped device. **f** The stabilized photocurrents of the pristine device and the PEO-doped device at the maximum power point. Reprinted with permission from ref. [166] Copyright 2020 American Chemical Society

recombination at the interfaces and in bulk have to be addressed for producing high-performance PSCs.

Acknowledgments The authors acknowledge the National Science Foundation (ECCS/EPMD1903303) and Air Force Office of Scientific Research (through the Organic Materials Chemistry Program, Grant Number: FA9550-15-1-0292, Program Manager, Dr. Kenneth Caster) for financial supports.

References

- S.D. Stranks, H.J. Snaith, Metal-halide perovskites for photovoltaic and light-emitting devices. Nat. Nanotechnol. 10(5), 391–402 (2015)
- B. Wang, X. Xiao, T. Chen, Perovskite photovoltaics: a highefficiency newcomer to the solar cell family. Nanoscale 6(21), 12287–12297 (2014)







- N.G. Park, Perovskite solar cells: an emerging photovoltaic technology. Mater. Today 18(2), 65–72 (2015)
- H.S. Jung, N.G. Park, Perovskite solar cells: from materials to devices. Small 11(1), 10–25 (2015)
- A. Kojima, K. Teshima, Y. Shirai, T. Miyasaka, Organometal halide perovskites as visible-light sensitizers for photovoltaic cells. J. Am. Chem. Soc. 131(17), 6050–6051 (2009)
- H. Kim, K.G. Lim, T.W. Lee, Planar heterojunction organometal halide perovskite solar cells: roles of interfacial layers. Energy Environ. Sci. 9(1), 12–30 (2016)
- J. Seo, J.H. Noh, S.I. Seok, Rational strategies for efficient perovskite solar cells. Acc. Chem. Res. 49(3), 562–572 (2016)
- S. Kazim, M.K. Nazeeruddin, M. Grätzel, S. Ahmad, Perovskite as light harvester: a game changer in photovoltaics. Angew. Chem. Int. Ed. 53(11), 2812–2824 (2014)
- P.P. Boix, K. Nonomura, N. Mathews, S.G. Mhaisalkar, Current progress and future perspectives for organic/inorganic perovskite solar cells. Mater. Today 17(1), 16–23 (2014)
- G. Mathiazhagan, L. Wagner, S. Bogati, K.B.Y. Ünal, D. Bogachuk, T. Kroyer, S. Mastroianni, A. Hinsch, Double-mesoscopic hole-transport-material-free perovskite solar cells: overcoming charge-transport limitation by sputtered ultrathin Al₂O₃ isolating layer. ACS Appl. Nano Mater. 3(3), 2463–2471 (2020)
- J. Liu, D. Wang, K. Chen, J. Kang, J. Yang, J. Zhang, H. Zhang, Enhanced photovoltaic performance and reduced hysteresis in hole-conductor-free, printable mesoscopic perovskite solar cells based on melamine hydroiodide modified MAPbI₃. Sol. Energy 206, 548–554 (2020)
- Q. Chen, H. Zhou, Z. Hong, S. Luo, H.S. Duan, H.-H. Wang, Y. Liu, G. Li, Y. Yang, Planar heterojunction perovskite solar cells via vapor-assisted solution process. J. Am. Chem. Soc. 136(2), 622–625 (2014)
- Y.J. Jeon, S. Lee, R. Kang, J.E. Kim, J.S. Yeo, S.H. Lee, S.S. Kim, J.M. Yun, D.Y. Kim, Planar heterojunction perovskite solar cells with superior reproducibility. Sci. Rep. 4(1), 1–7 (2014)
- W. Xu, Y. Gao, W. Ming, F. He, J. Li, X.H. Zhu, F. Kang, J. Li, G. Wei, Suppressing defects-induced nonradiative recombination for efficient perovskite solar cells through green antisolvent engineering. Adv. Mater. 32(38), 2003965 (2020)
- W. Xu, L. Zheng, T. Zhu, L. Liu, X. Gong, Bulk heterojunction perovskite solar cells incorporated with Zn₂SnO₄ nanoparticles as the electron acceptors. ACS Appl. Mater. Interfaces 11(37), 34020–34029 (2019)
- X. Huang, K. Wang, C. Yi, T. Meng, X. Gong, Efficient perovskite hybrid solar cells by highly electrical conductive PEDOT: PSS hole transport layer. Adv. Energy Mater. 6(3), 1501773 (2016)
- C. Liu, K. Wang, P. Du, C. Yi, T. Meng, X. Gong, Efficient solution-processed bulk heterojunction perovskite hybrid solar cells. Adv. Energy Mater. 5(12), 1402024 (2015)
- K. Wang, C. Liu, C. Yi, L. Chen, J. Zhu, R. Weiss, X. Gong, Efficient perovskite hybrid solar cells via ionomer interfacial engineering. Adv. Funct. Mater. 25(44), 6875–6884 (2015)
- F. Serrano-Sanchez, J. Conesa, J. Rodrigues, C. Marini, J. Martínez, J. Alonso, Divalent chromium in the octahedral positions of the novel hybrid perovskites CH₃NH₃Pb_{1-x}Cr_x(Br, Cl)₃ (x = 0.25, 0.5): induction of narrow bands inside the bandgap. J. Alloys Compd. 821, 153414 (2020)
- H. Zhao, Y. Han, Z. Xu, C. Duan, S. Yang, S. Yuan, Z. Yang, Z. Liu, S. Liu, A novel anion doping for stable CsPbI₂Br perovskite solar cells with an efficiency of 15.56% and an open circuit voltage of 1.30 V. Adv. Energy Mater. 9(40), 1902279 (2019)
- T. Bu, X. Liu, Y. Zhou, J. Yi, X. Huang, L. Luo, J. Xiao, Z. Ku, Y. Peng, F. Huang, A novel quadruple-cation absorber for universal

- hysteresis elimination for high efficiency and stable perovskite solar cells. Energy Environ. Sci. **10**(12), 2509–2515 (2017)
- L. Calio, S. Kazim, M. Graetzel, S. Ahmad, Hole-transport materials for perovskite solar cells. Angew. Chem. Int. Ed. 55(47), 14522–14545 (2016)
- Z. Chen, B. Turedi, A.Y. Alsalloum, C. Yang, X. Zheng, I. Gereige, A. AlSaggaf, O.F. Mohammed, O.M. Bakr, Single-crystal MAPbI₃ perovskite solar cells exceeding 21% power conversion efficiency. ACS Energy Lett. 4(6), 1258–1259 (2019)
- H. Tsai, W. Nie, J.C. Blancon, C.C. Stoumpos, R. Asadpour, B. Harutyunyan, A.J. Neukirch, R. Verduzco, J.J. Crochet, S. Tretiak, High-efficiency two-dimensional Ruddlesden–Popper perovskite solar cells. Nature 536(7616), 312–316 (2016)
- L. Mao, W. Ke, L. Pedesseau, Y. Wu, C. Katan, J. Even, M.R. Wasielewski, C.C. Stoumpos, M.G. Kanatzidis, Hybrid Dion–Jacobson 2D lead iodide perovskites. J. Am. Chem. Soc. 140(10), 3775–3783 (2018)
- T.C. Sum, N. Mathews, Advancements in perovskite solar cells: photophysics behind the photovoltaics. Energy Environ. Sci. 7(8), 2518–2534 (2014)
- S. Luo, W.A. Daoud, Recent progress in organic–inorganic halide perovskite solar cells: mechanisms and material design. J. Mater. Chem. A 3(17), 8992–9010 (2015)
- M.A. Green, A. Ho-Baillie, H.J. Snaith, The emergence of perovskite solar cells. Nat. Photonics 8(7), 506–514 (2014)
- J. Albero, A.M. Asiri, H. García, Influence of the composition of hybrid perovskites on their performance in solar cells. J. Mater. Chem. A 4(12), 4353–4364 (2016)
- G. Giorgi, K. Yamashita, Organic–inorganic halide perovskites: an ambipolar class of materials with enhanced photovoltaic performances. J. Mater. Chem. A 3(17), 8981–8991 (2015)
- G.R. Kumar, A.D. Savariraj, S. Karthick, S. Selvam, B. Balamuralitharan, H.J. Kim, K.K. Viswanathan, M. Vijaykumar, K. Prabakar, Phase transition kinetics and surface binding states of methylammonium lead iodide perovskite. Phys. Chem. Chem. Phys. 18(10), 7284–7292 (2016)
- C.C. Stoumpos, M.G. Kanatzidis, The renaissance of halide perovskites and their evolution as emerging semiconductors. Acc. Chem. Res. 48(10), 2791–2802 (2015)
- R.H. Mitchell, M.D. Welch, A.R. Chakhmouradian, Nomenclature of the perovskite supergroup: a hierarchical system of classification based on crystal structure and composition. Mineral. Mag. 81(3), 411–461 (2017)
- C.C. Stoumpos, M.G. Kanatzidis, Halide perovskites: poor Man's high-performance semiconductors. Adv. Mater. 28(28), 5778– 5793 (2016)
- K. Wang, L. Zheng, T. Zhu, X. Yao, C. Yi, X. Zhang, Y. Cao, L. Liu, W. Hu, X. Gong, Efficient perovskite solar cells by hybrid perovskites incorporated with heterovalent neodymium cations. Nano Energy 61, 352–360 (2019)
- W. Xu, L. Zheng, X. Zhang, Y. Cao, T. Meng, D. Wu, L. Liu, W. Hu, X. Gong, Efficient perovskite solar cells fabricated by Co partially substituted hybrid perovskite. Adv. Energy Mater. 8(14), 1703178 (2018)
- P.P. Boix, S. Agarwala, T.M. Koh, N. Mathews, S.G. Mhaisalkar, Perovskite solar cells: beyond methylammonium lead iodide. J. Phys. Chem. Lett. 6(5), 898–907 (2015)
- D.H. Kang, N.G. Park, On the current–voltage hysteresis in perovskite solar cells: dependence on perovskite composition and methods to remove hysteresis. Adv. Mater. 31(34), 1805214 (2019)
- T. Zhu, Y. Yang, X. Gong, Recent advancements and challenges for low-toxicity perovskite materials. ACS Appl. Mater. Interfaces 12(24), 26776–26811 (2020)









- T. Meng, C. Yi, L. Liu, A. Karim, X. Gong, Enhanced thermoelectric properties of two-dimensional conjugated polymers. Emergent Mater. 1(1–2), 67–76 (2018)
- T. Zhu, L. Zheng, C. Yi, T. Yu, Y. Cao, L. Liu, X. Gong, Twodimensional conjugated polymeric nanocrystals for organic electronics. ACS Appl. Electron. Mater. 1(8), 1458–1464 (2019)
- Y. Zhou, Y. Zhao, Chemical stability and instability of inorganic halide perovskites. Energy Environ. Sci. 12(5), 1495–1511 (2019)
- B.W. Park, S.I. Seok, Intrinsic instability of inorganic-organic hybrid halide perovskite materials. Adv. Mater. 31(20), 1805337 (2019)
- Y. Fu, M.P. Hautzinger, Z. Luo, F. Wang, D. Pan, M.M. Aristov, I.A. Guzei, A. Pan, X. Zhu, S. Jin, Incorporating large A cations into lead iodide perovskite cages: relaxed Goldschmidt tolerance factor and impact on exciton–phonon interaction. ACS Cent. Sci. 5(8), 1377–1386 (2019)
- 45. T. Matsui, T. Yamamoto, T. Nishihara, R. Morisawa, T. Yokoyama, T. Sekiguchi, T. Negami, Compositional engineering for thermally stable, highly efficient perovskite solar cells exceeding 20% power conversion efficiency with 85 ° C/85% 1000 h stability. Adv. Mater. 31(10), 1806823 (2019)
- N. Li, Z. Zhu, C.C. Chueh, H. Liu, B. Peng, A. Petrone, X. Li, L. Wang, A.K.Y. Jen, Mixed cation FA_xPEA_{1-x}PbI₃ with enhanced phase and ambient stability toward high-performance perovskite solar cells. Adv. Energy Mater. 7(1), 1601307 (2017)
- T. Leijtens, K. Bush, R. Cheacharoen, R. Beal, A. Bowring, M.D. McGehee, Towards enabling stable lead halide perovskite solar cells; interplay between structural, environmental, and thermal stability. J. Mater. Chem. A 5(23), 11483–11500 (2017)
- Q. Han, S.H. Bae, P. Sun, Y.T. Hsieh, Y. Yang, Y.S. Rim, H. Zhao, Q. Chen, W. Shi, G. Li, Single crystal formamidinium lead iodide (FAPbI₃): insight into the structural, optical, and electrical properties. Adv. Mater. 28(11), 2253–2258 (2016)
- Y. Li, F.Z. Liu, M. Waqas, T.L. Leung, H.W. Tam, X.Q. Lan, B. Tu, W. Chen, A.B. Djurišić, Z.B. He, Formamidinium-based lead halide perovskites: structure, properties, and fabrication methodologies. Small Methods 2(7), 1700387 (2018)
- T.M. Koh, K. Fu, Y. Fang, S. Chen, T. Sum, N. Mathews, S.G. Mhaisalkar, P.P. Boix, T. Baikie, Formamidinium-containing metal-halide: an alternative material for near-IR absorption perovskite solar cells. J. Phys. Chem. C 118(30), 16458–16462 (2014)
- S. Pang, H. Hu, J. Zhang, S. Lv, Y. Yu, F. Wei, T. Qin, H. Xu, Z. Liu, G. Cui, NH₂CH=NH₂PbI₃: an alternative organolead iodide perovskite sensitizer for mesoscopic solar cells. Chem. Mater. 26(3), 1485–1491 (2014)
- W.S. Yang, J.H. Noh, N.J. Jeon, Y.C. Kim, S. Ryu, J. Seo, S.I. Seok, High-performance photovoltaic perovskite layers fabricated through intramolecular exchange. Science 348(6240), 1234–1237 (2015)
- G.E. Eperon, S.D. Stranks, C. Menelaou, M.B. Johnston, L.M. Herz, H.J. Snaith, Formamidinium lead trihalide: a broadly tunable perovskite for efficient planar heterojunction solar cells. Energy Environ. Sci. 7(3), 982–988 (2014)
- G.S. Shin, Y. Zhang, N.-G. Park, Stability of precursor solution for perovskite solar cell: mixture (FAI+ PbI₂) versus synthetic FAPbI₃ crystal. ACS Appl. Mater. Interfaces 12(13), 15167– 15174 (2020)
- G.E. Eperon, G.M. Paterno, R.J. Sutton, A. Zampetti, A.A. Haghighirad, F. Cacialli, H.J. Snaith, Inorganic caesium lead iodide perovskite solar cells. J. Mater. Chem. A 3(39), 19688– 19695 (2015)
- M. Kulbak, D. Cahen, G. Hodes, How important is the organic part of lead halide perovskite photovoltaic cells? Efficient CsPbBr₃ cells. J. Phys. Chem. Lett. 6(13), 2452–2456 (2015)
- Q. Ma, S. Huang, X. Wen, M.A. Green, A.W. Ho-Baillie, Hole transport layer free inorganic CsPbIBr₂ perovskite solar cell by

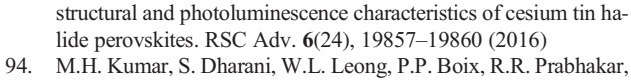
- dual source thermal evaporation. Adv. Energy Mater. **6**(7), 1502202 (2016)
- J. Liang, C. Wang, Y. Wang, Z. Xu, Z. Lu, Y. Ma, H. Zhu, Y. Hu, C. Xiao, X. Yi, All-inorganic perovskite solar cells. J. Am. Chem. Soc. 138(49), 15829–15832 (2016)
- X. Liu, J. Han, Y. Li, B. Cao, C. Sun, H. Yin, Y. Shi, M. Jin, C. Liu, M. Sun, Ultrafast carrier dynamics in all-inorganic CsPbBr₃ perovskite across the pressure-induced phase transition. Opt. Express 27(16), A995–A1003 (2019)
- H. Chen, S. Xiang, W. Li, H. Liu, L. Zhu, S. Yang, Inorganic perovskite solar cells: a rapidly growing field. Sol. RRL 2(2), 1700188 (2018)
- K. Miyata, T.L. Atallah, X.Y. Zhu, Lead halide perovskites: crystal-liquid duality, phonon glass electron crystals, and large polaron formation. Sci. Adv. 3(10), e1701469 (2017)
- J. Tian, J. Wang, Q. Xue, T. Niu, L. Yan, Z. Zhu, N. Li, C.J. Brabec, H.L. Yip, Y. Cao, Composition engineering of allinorganic perovskite film for efficient and operationally stable solar cells. Adv. Funct. Mater. 30(28), 2001764 (2020)
- N. Pellet, P. Gao, G. Gregori, T.Y. Yang, M.K. Nazeeruddin, J. Maier, M. Grätzel, Mixed-organic-cation perovskite photovoltaics for enhanced solar-light harvesting. Angew. Chem. Int. Ed. 53(12), 3151–3157 (2014)
- 64. J. Liu, Y. Shirai, X. Yang, Y. Yue, W. Chen, Y. Wu, A. Islam, L. Han, High-quality mixed-organic-cation perovskites from a phase-pure non-stoichiometric intermediate (FAI)_{1-x}-PbI₂ for solar cells. Adv. Mater. 27(33), 4918–4923 (2015)
- N.J. Jeon, J.H. Noh, W.S. Yang, Y.C. Kim, S. Ryu, J. Seo, S.I. Seok, Compositional engineering of perovskite materials for highperformance solar cells. Nature 517(7535), 476–480 (2015)
- D. Bi, W. Tress, M.I. Dar, P. Gao, J. Luo, C. Renevier, K. Schenk, A. Abate, F. Giordano, J.-P.C. Baena, Efficient luminescent solar cells based on tailored mixed-cation perovskites. Sci. Adv. 2(1), e1501170 (2016)
- H. Choi, J. Jeong, H.B. Kim, S. Kim, B. Walker, G.H. Kim, J.Y. Kim, Cesium-doped methylammonium lead iodide perovskite light absorber for hybrid solar cells. Nano Energy 7, 80–85 (2014)
- J.W. Lee, D.H. Kim, H.S. Kim, S.W. Seo, S.M. Cho, N.G. Park, Formamidinium and cesium hybridization for photo-and moisture-stable perovskite solar cell. Adv. Energy Mater. 5(20), 1501310 (2015)
- C. Yi, J. Luo, S. Meloni, A. Boziki, N. Ashari-Astani, C. Grätzel, S.M. Zakeeruddin, U. Röthlisberger, M. Grätzel, Entropic stabilization of mixed A-cation ABX₃ metal halide perovskites for high performance perovskite solar cells. Energy Environ. Sci. 9(2), 656–662 (2016)
- W.S. Yang, B.W. Park, E.H. Jung, N.J. Jeon, Y.C. Kim, D.U. Lee, S.S. Shin, J. Seo, E.K. Kim, J.H. Noh, Iodide management in formamidinium-lead-halide-based perovskite layers for efficient solar cells. Science 356(6345), 1376–1379 (2017)
- J.M. Frost, K.T. Butler, F. Brivio, C.H. Hendon, M. Van Schilfgaarde, A. Walsh, Atomistic origins of high-performance in hybrid halide perovskite solar cells. Nano Lett. 14(5), 2584– 2590 (2014)
- B. Kim, S.I. Seok, Molecular aspects of organic cations affecting the humidity stability of perovskites. Energy Environ. Sci. 13(3), 805–820 (2020)
- M. Saliba, T. Matsui, J.Y. Seo, K. Domanski, J.-P. Correa-Baena, M.K. Nazeeruddin, S.M. Zakeeruddin, W. Tress, A. Abate, A. Hagfeldt, Cesium-containing triple cation perovskite solar cells: improved stability, reproducibility and high efficiency. Energy Environ. Sci. 9(6), 1989–1997 (2016)
- R. Singh, S. Sandhu, H. Yadav, J.J. Lee, Stable triple-cation (Cs⁺
 MA⁺–FA⁺) perovskite powder formation under ambient conditions for hysteresis-free high-efficiency solar cells. ACS Appl.
 Mater. Interfaces 11(33), 29941–29949 (2019)







- M. Saliba, T. Matsui, K. Domanski, J.Y. Seo, A. Ummadisingu, S.M. Zakeeruddin, J.-P. Correa-Baena, W.R. Tress, A. Abate, A. Hagfeldt, Incorporation of rubidium cations into perovskite solar cells improves photovoltaic performance. Science 354(6309), 206–209 (2016)
- Y. Hu, M.F. AygÜler, M.L. Petrus, T. Bein, P. Docampo, Impact of rubidium and cesium cations on the moisture stability of multiple-cation mixed-halide perovskites. ACS Energy Lett. 2(10), 2212–2218 (2017)
- H.J. Snaith, Present status and future prospects of perovskite photovoltaics. Nat. Mater. 17(5), 372–376 (2018)
- Q. Chen, N. De Marco, Y.M. Yang, T.B. Song, C.C. Chen, H. Zhao, Z. Hong, H. Zhou, Y. Yang, Under the spotlight: the organic–inorganic hybrid halide perovskite for optoelectronic applications. Nano Today 10(3), 355–396 (2015)
- D. Mitzi, S. Wang, C. Feild, C. Chess, A. Guloy, Conducting layered organic-inorganic halides containing
 10>-oriented perovskite sheets. Science 267(5203), 1473–1476 (1995)
- D.B. Mitzi, C. Feild, W. Harrison, A. Guloy, Conducting tin halides with a layered organic-based perovskite structure. Nature 369(6480), 467–469 (1994)
- Y. Dang, Y. Zhou, X. Liu, D. Ju, S. Xia, H. Xia, X. Tao, Formation of hybrid perovskite tin iodide single crystals by topseeded solution growth. Angew. Chem. Int. Ed. 55(10), 3447– 3450 (2016)
- F. Hao, C.C. Stoumpos, D.H. Cao, R.P. Chang, M.G. Kanatzidis, Lead-free solid-state organic–inorganic halide perovskite solar cells. Nat. Photonics 8(6), 489–494 (2014)
- F. Hao, C.C. Stoumpos, P. Guo, N. Zhou, T.J. Marks, R.P. Chang, M.G. Kanatzidis, Solvent-mediated crystallization of CH₃NH₃SnI₃ films for heterojunction depleted perovskite solar cells. J. Am. Chem. Soc. 137(35), 11445–11452 (2015)
- P. Zhu, C. Chen, S. Gu, R. Lin, J. Zhu, CsSnI₃ solar cells via an evaporation-assisted solution method. Sol. RRL 2(4), 1700224 (2018)
- W. Ke, C.C. Stoumpos, I. Spanopoulos, L. Mao, M. Chen, M.R. Wasielewski, M.G. Kanatzidis, Efficient lead-free solar cells based on hollow {en} MASnI₃ perovskites. J. Am. Chem. Soc. 139(41), 14800–14806 (2017)
- W. Ke, C.C. Stoumpos, M.G. Kanatzidis, "Unleaded" perovskites: status quo and future prospects of tin-based perovskite solar cells. Adv. Mater. 31(47), 1803230 (2019)
- C.C. Stoumpos, C.D. Malliakas, M.G. Kanatzidis, Semiconducting tin and lead iodide perovskites with organic cations: phase transitions, high mobilities, and near-infrared photoluminescent properties. Inorg. Chem. 52(15), 9019–9038 (2013)
- D. Mitzi, K. Liang, Synthesis, resistivity, and thermal properties of the cubic perovskite NH₂CH=NH₂SnI₃and related systems. J. Solid State Chem. 134(2), 376–381 (1997)
- F. Wang, J. Ma, F. Xie, L. Li, J. Chen, J. Fan, N. Zhao, Organic cation-dependent degradation mechanism of organotin halide perovskites. Adv. Funct. Mater. 26(20), 3417–3423 (2016)
- N.K. Noel, S.D. Stranks, A. Abate, C. Wehrenfennig, S. Guarnera, A.A. Haghighirad, A. Sadhanala, G.E. Eperon, S.K. Pathak, M.B. Johnston, Lead-free organic–inorganic tin halide perovskites for photovoltaic applications. Energy Environ. Sci. 7(9), 3061–3068 (2014)
- T.M. Koh, T. Krishnamoorthy, N. Yantara, C. Shi, W.L. Leong, P.P. Boix, A.C. Grimsdale, S.G. Mhaisalkar, N. Mathews, Formamidinium tin-based perovskite with low E_g for photovoltaic applications. J. Mater. Chem. A 3(29), 14996–15000 (2015)
- S.J. Lee, S.S. Shin, Y.C. Kim, D. Kim, T.K. Ahn, J.H. Noh, J. Seo, S.I. Seok, Fabrication of efficient formamidinium tin iodide perovskite solar cells through SnF₂-pyrazine complex. J. Am. Chem. Soc. 138(12), 3974–3977 (2016)



93. L. Peedikakkandy, P. Bhargava, Composition dependent optical,

- M.H. Kumar, S. Dharani, W.L. Leong, P.P. Boix, R.R. Prabhakar, T. Baikie, C. Shi, H. Ding, R. Ramesh, M. Asta, Lead-free halide perovskite solar cells with high photocurrents realized through vacancy modulation. Adv. Mater. 26(41), 7122–7127 (2014)
- L.Y. Huang, W.R. Lambrecht, Electronic band structure, phonons, and exciton binding energies of halide perovskites CsSnCl₃, CsSnBr₃, and CsSnI₃. Phys. Rev. B 88(16), 165203 (2013)
- L.Y. Huang, W.R. Lambrecht, Lattice dynamics in perovskite halides CsSnX₃ with X = I, Br, Cl. Phys. Rev. B 90(19), 195201 (2014)
- N. Wang, Y. Zhou, M.G. Ju, H.F. Garces, T. Ding, S. Pang, X.C. Zeng, N.P. Padture, X.W. Sun, Heterojunction-depleted lead-free perovskite solar cells with coarse-grained B-γ-CsSnI₃ thin films. Adv. Energy Mater. 6(24), 1601130 (2016)
- Y. Ogomi, A. Morita, S. Tsukamoto, T. Saitho, N. Fujikawa, Q. Shen, T. Toyoda, K. Yoshino, S.S. Pandey, T. Ma, CH₃NH₃Sn_xPb_(1-x)I₃ perovskite solar cells covering up to 1060 nm. J. Phys. Chem. Lett. 5(6), 1004–1011 (2014)
- F. Hao, C.C. Stoumpos, R.P. Chang, M.G. Kanatzidis, Anomalous band gap behavior in mixed Sn and Pb perovskites enables broadening of absorption spectrum in solar cells. J. Am. Chem. Soc. 136(22), 8094–8099 (2014)
- F. Zuo, S.T. Williams, P.W. Liang, C.C. Chueh, C.Y. Liao, A.K.Y. Jen, Binary-metal perovskites toward high-performance planar-heterojunction hybrid solar cells. Adv. Mater. 26(37), 6454–6460 (2014)
- 101. Q. Shen, Y. Ogomi, J. Chang, T. Toyoda, K. Fujiwara, K. Yoshino, K. Sato, K. Yamazaki, M. Akimoto, Y. Kuga, Optical absorption, charge separation and recombination dynamics in Sn/Pb cocktail perovskite solar cells and their relationships to photovoltaic performances. J. Mater. Chem. A 3(17), 9308–9316 (2015)
- A. Mancini, P. Quadrelli, C. Milanese, M. Patrini, G. Guizzetti, L. Malavasi, CH₃NH₃Sn_xPb_{1-x}Br₃ hybrid perovskite solid solution: synthesis, structure, and optical properties. Inorg. Chem. 54(18), 8893–8895 (2015)
- 103. M.T. Klug, A. Osherov, A.A. Haghighirad, S.D. Stranks, P.R. Brown, S. Bai, J.T.-W. Wang, X. Dang, V. Bulović, H.J. Snaith, Tailoring metal halide perovskites through metal substitution: influence on photovoltaic and material properties. Energy Environ. Sci. 10(1), 236–246 (2017)
- 104. Y. Liu, Z. Yang, D. Cui, X. Ren, J. Sun, X. Liu, J. Zhang, Q. Wei, H. Fan, F. Yu, Two-inch-sized perovskite CH₃NH₃PbX₃ (X = Cl, Br, I) crystals: growth and characterization. Adv. Mater. 27(35), 5176–5183 (2015)
- S. Ryu, J.H. Noh, N.J. Jeon, Y.C. Kim, W.S. Yang, J. Seo, S.I. Seok, Voltage output of efficient perovskite solar cells with high open-circuit voltage and fill factor. Energy Environ. Sci. 7(8), 2614–2618 (2014)
- R. Sheng, A. Ho-Baillie, S. Huang, S. Chen, X. Wen, X. Hao, M.A. Green, Methylammonium lead bromide perovskite-based solar cells by vapor-assisted deposition. J. Phys. Chem. C 119(7), 3545–3549 (2015)
- C.G. Wu, C.H. Chiang, S.H. Chang, A perovskite cell with a record-high-V_{oc} of 1.61 V based on solvent annealed CH₃NH₃PbBr₃/ICBA active layer. Nanoscale 8(7), 4077–4085 (2016)
- J.H. Noh, S.H. Im, J.H. Heo, T.N. Mandal, S.I. Seok, Chemical management for colorful, efficient, and stable inorganic-organic hybrid nanostructured solar cells. Nano Lett. 13(4), 1764–1769 (2013)
- M. Faghihnasiri, M. Izadifard, M.E. Ghazi, DFT study of mechanical properties and stability of cubic methylammonium lead halide









emergent mater. (2020) 3:727-750

- perovskites ($CH_3NH_3PbX_3$, X = I, Br, Cl). J. Phys. Chem. C **121**(48), 27059–27070 (2017)
- E. Mosconi, P. Umari, F. De Angelis, Electronic and optical properties of MAPbX₃ perovskites (X = I, Br, Cl): a unified DFT and GW theoretical analysis. Phys. Chem. Chem. Phys. 18(39), 27158–27164 (2016)
- B. Brunetti, C. Cavallo, A. Ciccioli, G. Gigli, A. Latini, On the thermal and thermodynamic (in) stability of methylammonium lead halide perovskites. Sci. Rep. 6, 31896 (2016)
- M.I. Saidaminov, A.L. Abdelhady, B. Murali, E. Alarousu, V.M. Burlakov, W. Peng, I. Dursun, L. Wang, Y. He, G. Maculan, High-quality bulk hybrid perovskite single crystals within minutes by inverse temperature crystallization. Nat. Commun. 6(1), 1–6 (2015)
- E. Edri, S. Kirmayer, D. Cahen, G. Hodes, High open-circuit voltage solar cells based on organic-inorganic lead bromide perovskite. J. Phys. Chem. Lett. 4(6), 897–902 (2013)
- J.H. Heo, D.H. Song, S.H. Im, Planar CH₃NH₃PbBr₃ hybrid solar cells with 10.4% power conversion efficiency, fabricated by controlled crystallization in the spin-coating process. Adv. Mater. 26(48), 8179–8183 (2014)
- S.T. Williams, F. Zuo, C.C. Chueh, C.Y. Liao, P.-W. Liang, A.K.Y. Jen, Role of chloride in the morphological evolution of organo-lead halide perovskite thin films. ACS Nano 8(10), 10640–10654 (2014)
- H. Yu, F. Wang, F. Xie, W. Li, J. Chen, N. Zhao, The role of chlorine in the formation process of "CH₃NH₃PbI_{3-x}Cl_x" perovskite. Adv. Funct. Mater. 24(45), 7102–7108 (2014)
- Q. Chen, H. Zhou, Y. Fang, A.Z. Stieg, T.B. Song, H.H. Wang, X. Xu, Y. Liu, S. Lu, J. You, The optoelectronic role of chlorine in CH₃NH₃PbI₃(Cl)-based perovskite solar cells. Nat. Commun. 6, 7269 (2015)
- S.D. Stranks, G.E. Eperon, G. Grancini, C. Menelaou, M.J. Alcocer, T. Leijtens, L.M. Herz, A. Petrozza, H.J. Snaith, Electron-hole diffusion lengths exceeding 1 micrometer in an organometal trihalide perovskite absorber. Science 342(6156), 341–344 (2013)
- 119. C. Cao, C. Zhang, J. Yang, J. Sun, S. Pang, H. Wu, R. Wu, Y. Gao, C. Liu, Iodine and chlorine element evolution in CH₃NH₃PbI_{3-x}Cl_x thin films for highly efficient planar heterojunction perovskite solar cells. Chem. Mater. 28(8), 2742–2749 (2016)
- S. Colella, E. Mosconi, P. Fedeli, A. Listorti, F. Gazza, F. Orlandi, P. Ferro, T. Besagni, A. Rizzo, G. Calestani, MAPbI_{3-x}Cl_x mixed halide perovskite for hybrid solar cells: the role of chloride as dopant on the transport and structural properties. Chem. Mater. 25(22), 4613–4618 (2013)
- Z. Cheng, J. Lin, Layered organic–inorganic hybrid perovskites: structure, optical properties, film preparation, patterning and templating engineering. CrystEngComm 12(10), 2646–2662 (2010)
- 122. M. Zhang, M. Lyu, H. Yu, J.H. Yun, Q. Wang, L. Wang, Stable and low-cost mesoscopic CH₃NH₃PbI₂Br perovskite solar cells by using a thin poly (3-hexylthiophene) layer as a hole transporter. Chem. Eur. J. 21(1), 434–439 (2015)
- B. Suarez, V. Gonzalez-Pedro, T.S. Ripolles, R.S. Sanchez, L. Otero, I. Mora-Sero, Recombination study of combined halides (Cl, Br, I) perovskite solar cells. J. Phys. Chem. Lett. 5(10), 1628–1635 (2014)
- 124. W. Zhu, C. Bao, F. Li, T. Yu, H. Gao, Y. Yi, J. Yang, G. Fu, X. Zhou, Z. Zou, A halide exchange engineering for CH₃NH₃PbI₃ xBr_x perovskite solar cells with high performance and stability. Nano Energy 19, 17–26 (2016)
- S. Aharon, B.E. Cohen, L. Etgar, Hybrid lead halide iodide and lead halide bromide in efficient hole conductor free perovskite solar cell. J. Phys. Chem. C 118(30), 17160–17165 (2014)

 E. Edri, S. Kirmayer, M. Kulbak, G. Hodes, D. Cahen, Chloride inclusion and hole transport material doping to improve methyl ammonium lead bromide perovskite-based high open-circuit voltage solar cells. J. Phys. Chem. Lett. 5(3), 429–433 (2014)

749

- Y. Tidhar, E. Edri, H. Weissman, D. Zohar, G. Hodes, D. Cahen, B. Rybtchinski, S. Kirmayer, Crystallization of methyl ammonium lead halide perovskites: implications for photovoltaic applications. J. Am. Chem. Soc. 136(38), 13249–13256 (2014)
- 128. B.W. Park, B. Philippe, X. Zhang, H. Rensmo, G. Boschloo, E.M. Johansson, Bismuth based hybrid perovskites A₃Bi₂I₉ (A: methylammonium or cesium) for solar cell application. Adv. Mater. 27(43), 6806–6813 (2015)
- 129. E.T. McClure, M.R. Ball, W. Windl, P.M. Woodward, Cs₂AgBiX₆ (X = Br, Cl): new visible light absorbing, lead-free halide perovskite semiconductors. Chem. Mater. 28(5), 1348– 1354 (2016)
- B. Saparov, F. Hong, J.P. Sun, H.S. Duan, W. Meng, S. Cameron, I.G. Hill, Y. Yan, D.B. Mitzi, Thin-film preparation and characterization of Cs₃Sb₂I₉: a lead-free layered perovskite semiconductor. Chem. Mater. 27(16), 5622–5632 (2015)
- D. Cortecchia, H.A. Dewi, J. Yin, A. Bruno, S. Chen, T. Baikie, P.P. Boix, M. Grätzel, S. Mhaisalkar, C. Soci, Lead-free MA₂CuCl_xBr_{4-x} hybrid perovskites. Inorg. Chem. 55(3), 1044– 1052 (2016)
- Y. Zheng, R. Su, Z. Xu, D. Luo, H. Dong, B. Jiao, Z. Wu, Q. Gong, R. Zhu, Perovskite solar cell towards lower toxicity: a theoretical study of physical lead reduction strategy. Sci. Bull. 64(17), 1255–1261 (2019)
- A. Abate, Perovskite solar cells go lead free. Joule 1(4), 659–664 (2017)
- R.L. Hoye, R.E. Brandt, A. Osherov, V. Stevanović, S.D. Stranks, M.W. Wilson, H. Kim, A.J. Akey, J.D. Perkins, R.C. Kurchin, Methylammonium bismuth iodide as a lead-free, stable hybrid organic–inorganic solar absorber. Chem. Eur. J. 22(8), 2605– 2610 (2016)
- 135. M. Lyu, J.H. Yun, M. Cai, Y. Jiao, P.V. Bernhardt, M. Zhang, Q. Wang, A. Du, H. Wang, G. Liu, Organic–inorganic bismuth (III)-based material: a lead-free, air-stable and solution-processable light-absorber beyond organolead perovskites. Nano Res. 9(3), 692–702 (2016)
- K. Eckhardt, V. Bon, J. Getzschmann, J. Grothe, F.M. Wisser, S. Kaskel, Crystallographic insights into (CH₃NH₃)₃(Bi₂I₉): a new lead-free hybrid organic—inorganic material as a potential absorber for photovoltaics. Chem. Commun. 52(14), 3058–3060 (2016)
- 137. Z. Yang, A. Surrente, K. Galkowski, N. Bruyant, D.K. Maude, A.A. Haghighirad, H.J. Snaith, P. Plochocka, R.J. Nicholas, Unraveling the exciton binding energy and the dielectric constant in single-crystal methylammonium lead triiodide perovskite. J. Phys. Chem. Lett. 8(8), 1851–1855 (2017)
- B. Hwang, J.-S. Lee, Lead-free, air-stable hybrid organicinorganic perovskite resistive switching memory with ultrafast switching and multilevel data storage. Nanoscale 10(18), 8578– 8584 (2018)
- 139. J.C. Dahl, W.T. Osowiecki, Y. Cai, J.K. Swabeck, Y. Bekenstein, M. Asta, E.M. Chan, A.P. Alivisatos, Probing the stability and band gaps of Cs₂AgInCl₆ and Cs₂AgSbCl₆ lead-free double perovskite nanocrystals. Chem. Mater. 31(9), 3134–3143 (2019)
- P.K. Kung, M.H. Li, P.Y. Lin, J.Y. Jhang, M. Pantaler, D.C. Lupascu, G. Grancini, P. Chen, Lead-free double perovskites for perovskite solar cells. Sol. RRL 4(2), 1900306 (2020)
- G. Volonakis, M.R. Filip, A.A. Haghighirad, N. Sakai, B. Wenger, H.J. Snaith, F. Giustino, Lead-free halide double perovskites via heterovalent substitution of noble metals. J. Phys. Chem. Lett. 7(7), 1254–1259 (2016)







- P. Huang, S. Kazim, M. Wang, S. Ahmad, Toward phase stability: Dion–Jacobson layered perovskite for solar cells. ACS Energy Lett. 4(12), 2960–2974 (2019)
- S. Ahmad, P. Fu, S. Yu, Q. Yang, X. Liu, X. Wang, X. Wang, X. Guo, C. Li, Dion-Jacobson phase 2D layered perovskites for solar cells with ultrahigh stability. Joule 3(3), 794–806 (2019)
- 144. F.C. Hanusch, E. Wiesenmayer, E. Mankel, A. Binek, P. Angloher, C. Fraunhofer, N. Giesbrecht, J.M. Feckl, W. Jaegermann, D. Johrendt, Efficient planar heterojunction perovskite solar cells based on formamidinium lead bromide. J. Phys. Chem. Lett. 5(16), 2791–2795 (2014)
- Y. Zhou, M. Yang, S. Pang, K. Zhu, N.P. Padture, Exceptional morphology-preserving evolution of formamidinium lead triiodide perovskite thin films via organic-cation displacement. J. Am. Chem. Soc. 138(17), 5535–5538 (2016)
- M.R. Leyden, M.V. Lee, S.R. Raga, Y. Qi, Large formamidinium lead trihalide perovskite solar cells using chemical vapor deposition with high reproducibility and tunable chlorine concentrations.
 J. Mater. Chem. A 3(31), 16097–16103 (2015)
- S. Wozny, M. Yang, A.M. Nardes, C.C. Mercado, S. Ferrere, M.O. Reese, W. Zhou, K. Zhu, Controlled humidity study on the formation of higher efficiency formamidinium lead triiodidebased solar cells. Chem. Mater. 27(13), 4814

 –4820 (2015)
- 148. S. Lv, S. Pang, Y. Zhou, N.P. Padture, H. Hu, L. Wang, X. Zhou, H. Zhu, L. Zhang, C. Huang, One-step, solution-processed formamidinium lead trihalide (FAPbI_(3-x)Cl_x) for mesoscopic perovskite–polymer solar cells. Phys. Chem. Chem. Phys. 16(36), 19206–19211 (2014)
- 149. T.S. Ripolles, K. Nishinaka, Y. Ogomi, Y. Miyata, S. Hayase, Efficiency enhancement by changing perovskite crystal phase and adding a charge extraction interlayer in organic amine freeperovskite solar cells based on cesium. Sol. Energy Mater. Sol. Cells 144, 532–536 (2016)
- Z. Li, M. Yang, J.S. Park, S.H. Wei, J.J. Berry, K. Zhu, Stabilizing perovskite structures by tuning tolerance factor: formation of formamidinium and cesium lead iodide solid-state alloys. Chem. Mater. 28(1), 284–292 (2016)
- T. Luo, Y. Zhang, Z. Xu, T. Niu, J. Wen, J. Lu, S. Jin, S. Liu, K. Zhao, Compositional control in 2D perovskites with alternating cations in the interlayer space for photovoltaics with efficiency over 18%. Adv. Mater. 31(44), 1903848 (2019)
- R. Yang, R. Li, Y. Cao, Y. Wei, Y. Miao, W.L. Tan, X. Jiao, H. Chen,
 L. Zhang, Q. Chen, Oriented quasi-2D perovskites for high performance optoelectronic devices. Adv. Mater. 30(51), 1804771 (2018)
- J. Shi, Y. Gao, X. Gao, Y. Zhang, J. Zhang, X. Jing, M. Shao, Fluorinated low-dimensional Ruddlesden–Popper perovskite solar cells with over 17% power conversion efficiency and improved stability. Adv. Mater. 31(37), 1901673 (2019)
- 154. H. Lai, B. Kan, T. Liu, N. Zheng, Z. Xie, T. Zhou, X. Wan, X. Zhang, Y. Liu, Y. Chen, Two-dimensional Ruddlesden–Popper perovskite with nanorod-like morphology for solar cells with

- efficiency exceeding 15%. J. Am. Chem. Soc. **140**(37), 11639–11646 (2018)
- H. Wang, C.C. Chan, M. Chu, J. Xie, S. Zhao, X. Guo, Q. Miao, K.S. Wong, K. Yan, J. Xu, Interlayer cross-linked 2D perovskite solar cell with uniform phase distribution and increased exciton coupling. Sol. RRL 4(4), 1900578 (2020)
- J. Zhou, Z. Ye, J. Hou, J. Wu, Y.Z. Zheng, X. Tao, Efficient ambient-air-stable HTM-free carbon-based perovskite solar cells with hybrid 2D–3D lead halide photoabsorbers. J. Mater. Chem. A 6(45), 22626–22635 (2018)
- X. Zhang, G. Wu, W. Fu, M. Qin, W. Yang, J. Yan, Z. Zhang, X. Lu, H. Chen, Orientation regulation of phenylethylammonium cation based 2D perovskite solar cell with efficiency higher than 11%. Adv. Energy Mater. 8(14), 1702498 (2018)
- 158. Y. Chen, Y. Sun, J. Peng, W. Zhang, X. Su, K. Zheng, T. Pullerits, Z. Liang, Tailoring organic cation of 2D air-stable organometal halide perovskites for highly efficient planar solar cells. Adv. Energy Mater. 7(18), 1700162 (2017)
- P. Cheng, Z. Xu, J. Li, Y. Liu, Y. Fan, L. Yu, D.-M. Smilgies, C. MÜller, K. Zhao, S.F. Liu, Highly efficient Ruddlesden–Popper halide perovskite PA₂MA₄Pb₅I₁₆ solar cells. ACS Energy Lett. 3(8), 1975–1982 (2018)
- K. Yao, X. Wang, Y.X. Xu, F. Li, L. Zhou, Multilayered perovskite materials based on polymeric-ammonium cations for stable large-area solar cell. Chem. Mater. 28(9), 3131–3138 (2016)
- W. Fu, H. Liu, X. Shi, L. Zuo, X. Li, A.K.Y. Jen, Tailoring the functionality of organic spacer cations for efficient and stable quasi-2D perovskite solar cells. Adv. Funct. Mater. 29(25), 1900221 (2019)
- 162. J. Rodríguez-Romero, B.C. Hames, P. Galar, A. Fakharuddin, I. Suarez, L. Schmidt-Mende, J.P. Martínez-Pastor, A. Douhal, I. Mora-Seró, E.M. Barea, Tuning optical/electrical properties of 2D/3D perovskite by the inclusion of aromatic cation. Phys. Chem. Chem. Phys. 20(48), 30189–30199 (2018)
- 163. C.M.M. Soe, C.C. Stoumpos, M. Kepenekian, B. Traoré, H. Tsai, W. Nie, B. Wang, C. Katan, R. Seshadri, A.D. Mohite, New type of 2D perovskites with alternating cations in the interlayer space, (C(NH₂)₃)(CH₃NH₃)_nPb_nI_{3n+1}: structure, properties, and photovoltaic performance. J. Am. Chem. Soc. 139(45), 16297–16309 (2017)
- M. Safdari, P.H. Svensson, M.T. Hoang, I. Oh, L. Kloo, J.M. Gardner, Layered 2D alkyldiammonium lead iodide perovskites: synthesis, characterization, and use in solar cells. J. Mater. Chem. A 4(40), 15638–15646 (2016)
- K. Wang, L. Zheng, T. Zhu, L. Liu, M.L. Becker, X. Gong, High performance perovskites solar cells by hybrid perovskites cocrystallized with poly (ethylene oxide). Nano Energy 67, 104229 (2020)
- 166. L. Zheng, K. Wang, T. Zhu, Y. Yang, R. Chen, K. Gu, C. Liu, X. Gong, High-performance perovskite solar cells by one-step self-assembled perovskite-polymer thin films. ACS Appl. Energy Mater. 3(6), 5902–5912 (2020)





